# Ultrasound-based estimates of cortical bone thickness and porosity are associated with non-traumatic fractures in postmenopausal women: A pilot study

J-G Minonzio, N Bochud, Q Vallet, D Ramiandrisoa, A Etcheto, K Briot, S Kolta, C Roux, P Laugier

# Ultrasound-based estimates of cortical bone thickness and porosity are associated with non-traumatic fractures in postmenopausal women: A pilot study

J-G Minonzio[1], N. Bochud[1,*], Q. Vallet[1], D. Ramiandrisoa[1], A. Etcheto[2], K. Briot[2,3], S. Kolta[2,3], C. Roux[2,3,4] and P. Laugier.[1]

[1] Sorbonne Université, CNRS, INSERM, Laboratoire d'Imagerie Biomédicale, F-75006, Paris, France

[2] INSERM UMR-1153, Paris, France

[3] Department of Rheumatology, Cochin Hospital, Assistance Publique - Hôpitaux de Paris, Paris, France

[4] Paris-Descartes University, Paris, France

## ABSTRACT

Recent ultrasound axial transmission techniques exploit the multimode waveguide response of long bones to yield estimates of cortical bone structure characteristics. This pilot cross-sectional study aimed to evaluate the performance at the one-third distal radius of a bidirectional axial transmission (BDAT) device to discriminate between fractured and non-fractured postmenopausal women. Cortical thickness (Ct.Th) and porosity (Ct.Po) estimates were obtained for 201 postmenopausal women, among whom 109 were non-fractured (62.6±7.8 years), 92 with one or more non-traumatic fractures (68.8±9.2 years), 17 with hip fractures (66.1±10.3 years), 32 with vertebral fractures (72.4±7.9 years), and 17 with wrist fractures (67.8±9.6 years). The areal bone mineral density (aBMD) was obtained using dual-energy X-ray absorptiometry (DXA) at the femur and spine. Femoral aBMD correlated weakly but significantly with Ct.Th ($R=0.23$, $p < 0.001$) and Ct.Po ($R=-0.15$, $p < 0.05$). Femoral aBMD and both ultrasound parameters were significantly different between the subgroup of all non-traumatic fractures combined and the control group ($p < 0.05$). The main findings were (i) that Ct.Po was discriminant for all non-traumatic fractures combined (odds ratio OR=1.39; area under the receiver operating characteristic curve AUC=0.71), for vertebral (OR=1.96; AUC=0.84) and wrist fractures (OR=1.80; AUC=0.71), while Ct.Th was discriminant for hip fractures only (OR=2.01; AUC=0.72); (ii) the demonstration of a significant association

between increased Ct.Po and vertebral and wrist fractures when these fractures were not associated with any measured aBMD variables; (iii) the association between increased Ct.Po and all non-traumatic fractures combined independently of aBMD neck; and (iv) the association between decreased Ct.Th and hip fractures independently of aBMD femur. BDAT variables showed comparable performance to that of aBMD neck with all types of fractures (OR=1.48; AUC=0.72) and that of aBMD femur with hip fractures (OR=2.21; AUC=0.70). If these results are confirmed in prospective studies, cortical BDAT measurements may be considered useful for assessing fracture risk in postmenopausal women.

*Keywords:* Cortical bone; osteoporosis; fracture discrimination; quantitative ultrasound; guided waves

## INTRODUCTION

Osteoporosis is a skeletal disease leading to bone fragility and increasing the risk of fractures.[1] Osteoporosis still remains a major public health problem worldwide[2] and it is therefore crucial to prevent severe fractures responsible for excess of mortality and considerable morbidity.[3,4] Patients are currently identified as having osteoporosis using dual-energy X-ray absorptiometry (DXA), assessing the areal bone mineral density (aBMD), directly measured at the main fracture sites, *i.e.*, hip and spine.[5] However, even though DXA remains the current gold standard, it is limited by the difficulty to set a threshold for fracture risk in the aBMD distribution.[6] Indeed, more than half of individuals who have low-trauma fractures have a T-score higher than the osteoporotic threshold defined by the World Health Organization (*i.e.*, T-score = -2.5).[7] Moreover, some diseases (diabetes, obesity) and treatments (glucocorticoids) are associated with an increase of fracture risk without an aBMD decrease.[8]

One of the reasons for the limitation of DXA is that it does not capture alterations of bone quality factors, namely the material and structural properties, and particularly those of cortical bone. Because of its projection technique, DXA is not able to separate the trabecular and cortical compartments. Impaired bone remodeling affects not only the trabecular compartment but also the cortical one, inducing thickness decrease and porosity increase.[9,10] Despite the crucial contribution of the cortical structure and microstructure to the whole bone mechanical competence, cortical bone was understudied for a long time.[11,12] Recent advances in high resolution imaging technology have driven growing recognition of the role of cortical microstructure in osteoporotic bone loss and fragility.[13]

In the past two decades, there has been a great deal of interest in new techniques to assess cortical bone. The high resolution peripheral quantitative computed tomography (HR-pQCT) technique has seen recent developments with regard to the assessment of cortical porosity.[10,14] Reference point indentation is proposed to assess the mechanical behavior of cortical bone.[15] There are currently different approaches for quantitative ultrasound (QUS) based on mechanical waves propagation, which possess intrinsic sensitivity to bone elastic and structural properties: transverse transmission measuring cortical bone at the one-third radius,[16] transverse transmission based on two longitudinal waves at the ultradistal radius,[17] pulse-echo techniques,[18] and axial transmission (AT),[19] specifically designed to measure cortical bone. Unlike HR-pQCT and reference point indentation, QUS has the advantages of portability, low cost, non-invasiveness, absence of radiation and no need for a radiographic technologist or designated room.[20]

In AT, transducers (emitters and receivers) aligned along the main bone axis are used to measure the speed of sound of waves guided along the cortex of a long bone, such as the radius or tibia.[21] With earlier approaches, analyses of AT signals were restricted to a single waveform, either the first arriving signal (FAS) or the fundamental flexural guided wave (FFGW). FAS velocity measured at the radius demonstrated ability to discriminate fracture cases from controls in postmenopausal women in numerous clinical studies, although, compared to DXA, FAS velocity has not shown superiority for fracture prediction.[22-25] The identification of the FFGW,[26] a slower waveform than FAS, whose dispersion characteristics (frequency-related phase velocity variations) are sensitive to cortical thickness for frequency thickness product lower than 0.5 MHz.mm,[27] has been a positive turning point for ultrasound cortical bone assessment. Indeed, while the precise bone properties reflected by FAS remain to be established, the FFGW velocity can be predicted with analytical models and thus an inverse problem approach allows inferring cortical thickness from measurements.[28] For a given waveguide and frequency bandwidth, multiple guided modes can coexist. These multiple modes contain more information than a single mode. Thus, the earlier analysis of AT signals, so far limited to a single waveform, has been extended to a full-waveform analysis. The problem is that, in the full waveform, distinguishing modes or their dispersion curves in recorded signals requires specific acquisition scheme or signal processing. Over the past years, the determination of guided modes and identification of cortical bone waveguide characteristics has sparked increased discussions of signal processing approaches,[29-32] modeling,[33-35] and inverse problem solving.[28,36-38]

Our group has developed the bidirectional axial transmission (BDAT) to this goal.[39] We recently showed that BDAT combined with an appropriate waveguide model allows the concurrent identification of cortical thickness and porosity of *ex vivo* human specimens.[40] In a pilot *in vivo* study, BDAT could identify cortical thickness nearly as accurately as conventional HR-pQCT.[41] Assessment of cortical thickness (Ct.Th) and porosity (Ct.Po) by BDAT may improve the identification of patients at high risk of fracture. Therefore, in this study, we compared *in vivo* measurements of spine and hip aBMD to cortical bone thickness and porosity assessed by BDAT in postmenopausal women with and without prior history of fracture. Our aim was to study whether these ultrasound parameters were associated with fracture.

## MATERIALS AND METHODS

### *Subjects*

Three hundred and one patients were recruited from the Rheumatology Department in Cochin Hospital, Paris, France, between April 2014 and November 2015. All of them were ambulatory female patients consulting for fracture risk assessment. The study has been approved by the ethical committee of the Committees for the protection of persons Ile de France III. A written informed consent was provided by the patients. The procedure of the study was in accordance with the Declaration of Helsinki. The fracture information, including site and time, was collected in medical records; and the diagnosis of vertebral fractures was confirmed based on spine imaging. Fractures were classified as traumatic and non-traumatic.

Five groups were created: a control group with patients without fracture (NF); patients with any non-traumatic fracture (F); patients with a hip fracture (HF); patients with one or several vertebral fractures (VF) and patients with a wrist fracture (WF).[42] Note that the groups were classified as follows: the HF group contained at least a hip fracture and potentially other

fractures, the VF group did not contain hip fractures and likewise the WF group did not contain hip and vertebral fractures. Exclusion criteria were: missing data ($n = 7$), patient suffering from a cancer ($n = 1$), two-hip replacement (no femoral DXA possible, $n = 9$), BMI < 15 ($n = 1$), and a history of traumatic fractures ($n = 33$). Thus, 250 postmenopausal women are the basis of this cross-sectional study. Note that among the VF group, 16 patients only had one vertebral fracture, 11 had two vertebral fractures and 5 had more than two vertebral fractures. The number of patients undergoing glucocorticoid treatment was as follows: 12 in the NF group and 12 in the F group.

*Ultrasonic measuring device*

The QUS device (Azalée, Paris, France) consists of three custom-made parts [Fig. 1(a)]. First, a 1-MHz BDAT probe adapted to forearm measurements (Vermon, Tours, France), which is composed of a linear array of piezocomposite elements divided in one array of 24 receivers surrounded by two arrays of 5 transmitters each. The probe has been specifically designed to measure guided waves propagating in two opposite directions and thus correct the bias on the guided modes wavenumbers induced by the inclination angle between the probe and the bone due to uneven overlying soft tissues.[39,43] Second, an electronic device used to transmit, receive and digitize signals (Althaïs, Tours, France). The electronic device allows exciting each transmitter successively with a wideband pulse (170 V, 1-MHz central frequency) of -6 dB power spectrum spanning the frequency range from 0.4 to 1.6 MHz. The received signals are 16 times averaged and then sampled with a 20 MHz frequency (1024 time samples, 12 bits). Third, a human machine interface (HMI, Bleu Solid, Paris, France), developed to display the spectrum of guided waves in quasi real-time (at a frame rate up to 4 Hz) and to guide the operator in finding during measurement the optimal position of the probe with respect to the main bone axis.

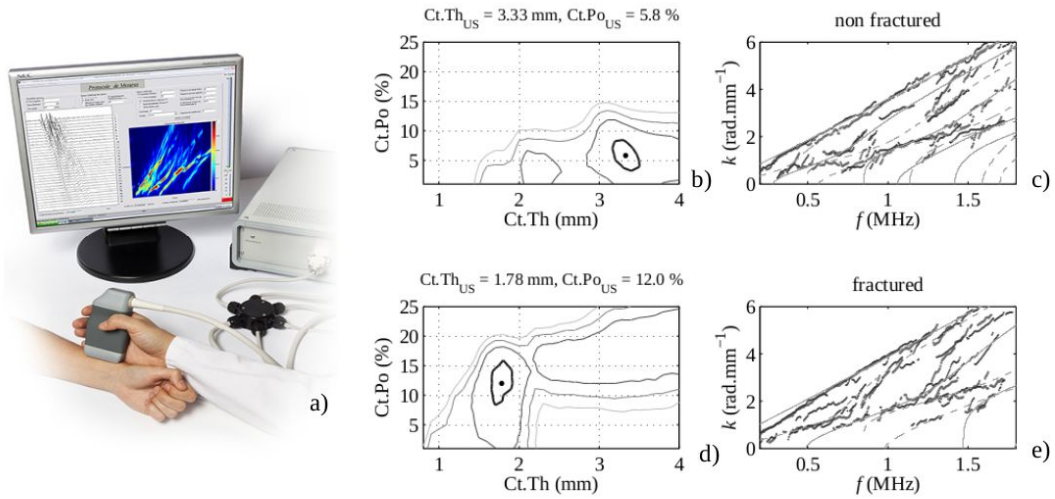


*Figure 1: (a) Illustration of the BDAT prototype device placed at the lateral one-third distal radius; (b)-(c) Example of the projected function (Eq. (2)) and guided mode wavenumbers vs frequency for a non-fractured patient; (d)-(e) Example of the projected function (Eq. (2)) and guided mode wavenumbers vs frequency for a patient with a non-traumatic shoulder fracture. The maxima (black dot) of the projected functions shown in (b) and (d) corresponds to the optimal theoretical waveguide models, whose guided modes are shown in (c) and (e) with continuous lines. Experimental guided mode wavenumbers are shown with dots. Contours in (b) and (d) correspond to values equal to the maximum of the projected function minus 0.1, 0.2, 0.3 and 0.4. The area delimited by the highest (thick) line can be interpreted as the measurement resolution, i.e., the ability of the measurement system to differentiate two close waveguide models. The resolution for the two ultrasound parameters is typically estimated to be about ±0.2 mm and ±2%.*

*Signal processing and cortical parameter identification*

Identification of cortical parameters is achieved through an approach that is an extension of the signal processing applied to extract the experimental guided mode wavenumbers from the maxima of the so-called Norm function.[29,44] The processing steps of the ultrasonic signals have been extensively described in our previous works.[41,44] Briefly, a singular value decomposition is applied at each frequency to the response matrix containing the temporal Fourier transforms of all transmitter-receiver signals. Signal-to-noise ratio enhancement is then achieved by retaining the singular vectors, denoted by $\boldsymbol{U}_n$, associated with the highest singular values, the lowest singular values being associated with noise. Finally, the projection of a variable testing vector onto the signal singular vector basis yields the Norm function. First, probe positioning is achieved by optimizing the *Norm* function, as it will be explained hereinafter in the measurement protocol section, which is defined as

$$Norm(f,k) = ||\boldsymbol{e}^{\text{test}}(k)||^2_{\boldsymbol{U}_n(f)}. \quad (1)$$

In this case, the testing vector $\boldsymbol{e}^{\text{test}}$ is a normalized attenuated plane wave.[44] This vector spans all waves measurable by the device corresponding to all frequencies $f$ and wavenumbers $k$ of the device bandwidth. Thus, each plane wave is associated with a pixel ($f$, $k$) of the *Norm* function, defined by the norm of the projected testing vector. The pixel value range reflects in a 0-1 scale the presence rate of the tested wave in the measured signals. The *Norm* function can thus be interpreted as an enhanced spatio-temporal Fourier transform.[29]

Second, in the case of waveguide parameters estimation, instead of spanning all measurable waves, the testing vectors are limited to the guided modes of a dedicated cortical bone waveguide model.[40] The waveguide model is a 2-D transverse isotropic free plate, parametrized in terms of thickness and elasticity.[37] Subsequently, we use an asymptotic homogenization approach to predict the mesoscopic stiffness coefficients from the microstructure, so that the elasticity of our model is parametrized in terms of porosity, assuming the bone matrix being spatially homogeneous and uniform among individuals.[45,46] The waveguide model corresponds to $M$ testing vectors depending on the guided mode wavenumbers, denoted by $k_m(f,Ct.Th,Ct.Po)$. Each pair of values (Ct.Th, Ct.Po) is associated with a projected value $Proj(Ct.Th,Ct.Po)$ defined by

$$Proj(Ct.Th,Ct.Po) = \frac{1}{f_{\max}-f_{\min}}\int_{f_{\min}}^{f_{\max}} \frac{1}{M}\sum_{m=1}^{M} ||\boldsymbol{e}^{\text{test}}(k_m(f,Ct.Th,Ct.Po))||^2_{\boldsymbol{U}_n(f)} df \quad (2)$$

where $f_{\min}$ and $f_{\max}$ are the frequency bandwidth limits. This equation corresponds to the weight of each testing vector for the whole frequency bandwidth. The highest magnitude of the projected function corresponds to the optimal pair of ultrasound parameters (denoted hereafter as $Ct.Th_{US}$ and $Ct.Po_{US}$) that allows reaching the best fit between the model and the experimental data. Representative examples of projected functions [Eq. (2)] are shown for a non-fractured [Fig. 1(b)] and a fractured [Fig. 1(d)] patient. The associated optimal waveguide model is shown in Figs. 1(c) and (e) together with the experimental guided modes obtained from the maxima of the *Norm* function [Eq. (1)].

*Measurement protocol*

A specific scanning methodology was carefully followed for measuring the patients. Measurements were done on the non-dominant forearm. When the non-dominant forearm undergoes a recent fracture, measurements were done on the contralateral arm. BDAT measurements were performed on a standardized region of interest (ROI), *i.e.*, the center of the probe was placed at the lateral side of the one-third distal radius (*i.e.*, 70 mm away from the radial styloid). The ROI length corresponds to the length of the receiver array (about two centimeters; the whole probe length being about five centimeters). The probe was placed in contact with the skin using ultrasonic gel for coupling (Aquasonic, Parker Labs Inc., Fairfield NJ, USA).

The measurement protocol consists of multiple series of ten acquisitions. By means of a visual inspection of the spectrum of guided waves displayed in real time by the HMI, once a correct probe position is found, ten successive acquisitions are recorded without moving the probe. The visual inspection relies on the following criteria: (i) the dispersion spectrum contains at least 3-4 guided modes (in particular, the low-order antisymmetric mode and higher-order modes, which are highly sensitive to the porosity and thickness of the waveguide, respectively); (ii) the measurement is stable (slight probe movements do not significantly alter the guided modes); and (iii) the guided modes measured in both directions are consistent. Next, to further ensure the measurement quality and compensate for this visual inspection, strict post-processing criteria were adopted to classify the measurement as a success or a failure.[40] In short, a series of ten acquisitions is considered as stable and is therefore retained if at least 7 acquisitions are successful, *i.e.*, provide the two parameters $Ct.Th_{US}$ and $Ct.Po_{US}$, and if the corresponding standard deviations are less than two heuristic thresholds fixed to 0.5 mm for $Ct.Th_{US}$ and 5% for $Ct.Po_{US}$. Each series corresponds to an intermediate repositioning of the probe. The measurement is considered as valid when at least three series are consistent, *i.e.*, when the differences of the values of each series are less than the two above mentioned thresholds. The final values of the identified waveguide parameters are set to the mean of the values of each successful series. The BDAT measurement on a patient typically lasts 5 to 10 minutes, a time lapse during which the patient is seated with the forearm in a still position on a table.

*Reproducibility*

The inter-operator reproducibility was evaluated by measuring 27 healthy subjects (21 to 55 years old, 16 males and 11 females) by two operators. A written informed consent was provided by the subjects, who were not part of the cohort of patients. Measurements were performed in a blinded fashion, *i.e.*, only one operator was present at the time. Three values were estimated to assess the reproducibility: the root mean square (RMS) average of the variance of duplicate measurements on the subjects, the intra-class correlation coefficient (ICC), and the standardized coefficient of variation (SCV), which is defined as the ratio of the RMS error by the range of measures given by four times the population standard deviation.[47]

*DXA reference measurements*

DXA measurements of the L2-L4 lumbar spine (aBMD spine), femoral neck (aBMD neck) and total femur (aBMD femur) were performed on patients using two systems of the same manufacturer: Delphi W and QDR 4500A (Hologic Bedford, MA, USA). The two devices have

been previously cross-calibrated. The patients were measured the same day by the two techniques, DXA and BDAT.

*Statistical analysis*

Statistical analyses have been performed using the open source programming language R and the Statistics and Machine Learning Toolbox provided by Matlab (MathWorks, Natick, MA USA). Continuous variables were presented as mean with standard deviation. Non-parametric tests were used. For each variable, a Wilcoxon-Mann-Whitney test was performed to determine whether the values were significantly different between the non-fractured group and any fractured group. Note that the statistical tests for QUS and DXA variables were achieved on variables adjusted for age, BMI and glucorticoid treatment. Spearman's rank correlation analysis was used to compare estimates of $Ct.Th_{US}$ and $Ct.Po_{US}$ with age, body mass index (BMI) and aBMD values. The level of statistical significance in both tests was determined at a *p*-value below 0.05.

To explore the association between the measured QUS and DXA variables and fragility fracture as a dependent variable, the odds ratios (ORs) were calculated using a binomial logistic regression analysis. ORs are expressed as increases in the estimated fracture risk per one standard deviation decrease for Ct.Th and aBMD or one standard deviation increase for Ct.Po. Receiver operator characteristic (ROC) curves were calculated and the area under the curve (AUC) was determined to examine for differences in the ability of DXA and QUS variables to separate between fracture participants and controls. Adjusted ORs and AUCs were computed with age, BMI, and glucocorticoid treatment as covariates. Various combinations of QUS parameters and aBMD values were also tested in multiple regression models to determine whether a combination of measured variables was able to improve fracture discrimination over a single variable. ROC analysis of the combined model was performed.

## RESULTS

*Inter-operator reproducibility*

The inter-operator results are shown in Fig. 2. Cortical thickness ranged from 2.8 to 3.9 mm while cortical porosity ranged from 3 to 12%. The RMS average of the variance of duplicate measurements were equal to 0.08 mm and 1.5% for cortical thickness and porosity, respectively. The ICC coefficients were equal to 0.90 and 0.59 for cortical thickness and porosity, respectively. The SCV lead to 4% and 10% for cortical thickness and porosity, respectively.

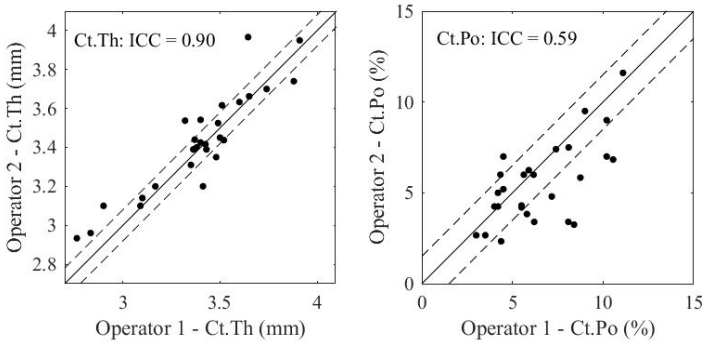


*Figure 2: Ct.Th (left) and Ct.Po (right) obtained by the two operators on the 27 healthy subjects of the reproducibility study. Dashed lines correspond to the RMS average of the variance of duplicate measurements, and the ICC is indicated in the upper left corner.*

*Measurement failure*

The ultrasonic measurement failed for 49 patients out of 250 (20% of the total cohort). Figure 3 depicts typical measurements for two patients, corresponding to a failure (BMI = 33 kg.m$^{-2}$, non-fractured) and a success (BMI = 18 kg.m$^{-2}$, fractured). Three panels are displayed for each measurement: (i) the time-domain signals (for one emission); (ii) the guided modes (*i.e.*, maxima of the *Norm* function); and (iii) the projected function (Eq. (2)). As can be observed, a failed measurement is generally associated with the following characteristics: (i) No proper wavefront can be recognized in the time-domain signals, whose waveform results in unexpected wave packets with high amplitude at relatively late arrivals (maybe due to scattering or waves guided in the soft tissue); (ii) poor guided modes; and (iii) a diverging objective function, for which there are no maxima within the explored domain of cortical thickness and porosity values.

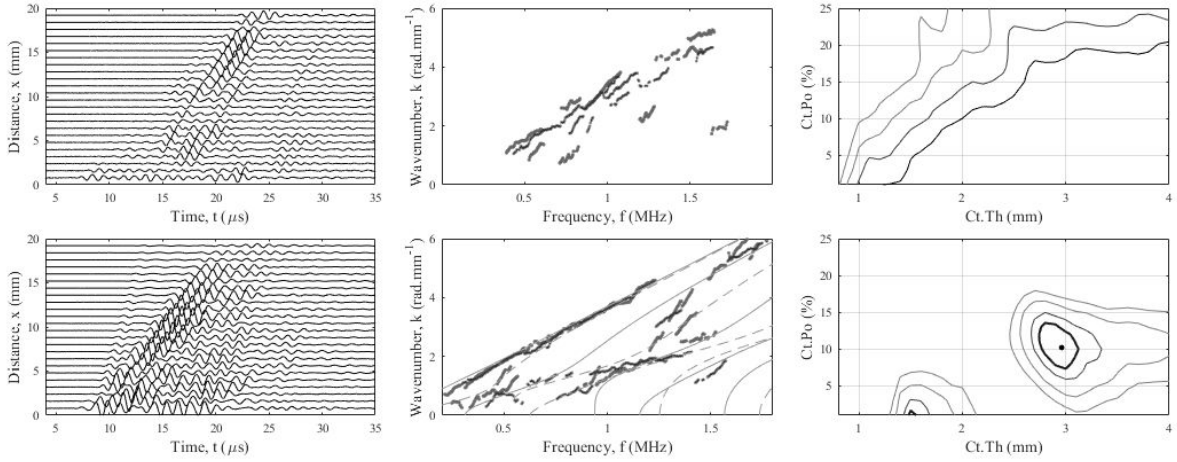


*Figure 3: Typical measurements for two patients, corresponding to a failure (upper panels) and a success (lower panels). Three panels are displayed for each measurement: (left) the time-domain signals (for one emission); (middle) the guided modes (i.e., maxima of the Norm function); and (right) the projected function (Eq. (2)).*

Figure 4 displays the failure rate as a function of BMI together with the BMI distribution. As depicted in Fig. 4(a), the failure rate increased with the BMI. For BMI larger than 28 kg.m$^{-2}$, the failure rate ranged between 55% and 75%. We did not observe any association between measurement failure and presence of fractures.

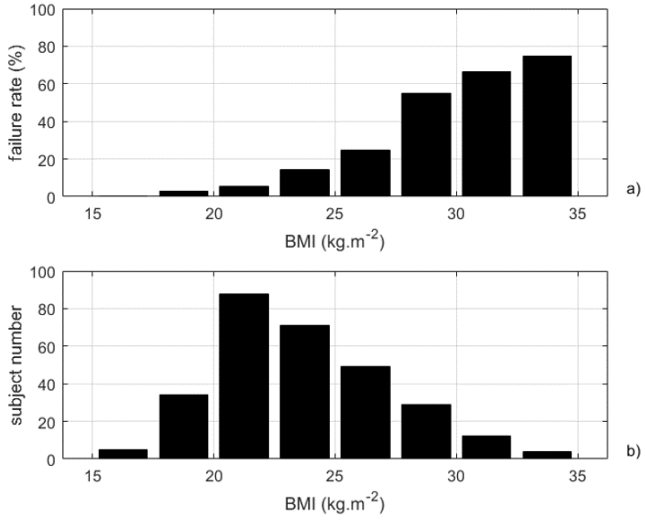


*Figure 4: (a) Failure rate (%) vs BMI (kg.m$^{-2}$) and (b) BMI distribution.*

*Patients' characteristics*

Among the 201 patients for whom the measurements were successful, 109 belong to the control group without fracture (NF), 92 to the group with non-traumatic fractures (F), 17 to the HF group, 32 to the VF group, and 17 to the WF group. Other fracture sites were: humerus, tibia, ankle and rib. The patients' descriptive characteristics are shown in Table 1. Mean age in all fractured groups was higher than in the non-fractured group and with the exception of the HF group the differences were all statistically significant. Note that the relatively young age of the hip fracture group is likely due to the fact that only ambulatory patients were measured with ultrasound.

*Table 1: Descriptive characteristics as mean and standard deviation (*p < 0.05 vs non-fractured group, **p < 0.01 vs non-fractured group, ***p < 0.001 vs non-fractured group). Note that the statistical tests for QUS and DXA variables were achieved on variables adjusted for age, BMI and glucorticoid treatment.*

| | NF (N=109) | F (N=92) | HF (N=17) | VF (N=32) | WF (N=17) |
|---|---|---|---|---|---|
| **Age (years)** | 62.6 (7.8) | 68.8 (9.2)*** | 66.1 (10.3) | 72.4 (7.9)*** | 67.8 (9.6)* |
| **Height (cm)** | 160.0 (6.1) | 158.2 (6.5)* | 160.0 (6.7) | 156.8 (6.4)* | 158.8 (8.3) |
| **Weight (kg)** | 58.8 (8.5) | 57.1 (8.8) | 59.8 (8.8) | 57.9 (9.3) | 56.7 (6.4) |
| **BMI ($kg.m^{-2}$)** | 22.9 (3.1) | 22.8 (3.1) | 23.4 (3.1) | 23.5 (3.5) | 22.5 (1.6) |
| **$Ct.Th_{US}$ (mm)** | 3.01 (0.44) | 2.83 (0.46)* | 2.61 (0.54)*** | 2.87 (0.41)* | 2.91 (0.37) |
| **$Ct.Po_{US}$ (%)** | 10.2 (3.0) | 11.6 (3.5)*** | 9.4 (2.8) | 12.8 (3.3)*** | 12.4 (2.8)*** |
| **aBMD neck ($g.cm^{-2}$)** | 0.661 (0.087) | 0.612 (0.068)*** | 0.607 (0.075)*** | 0.611 (0.069)* | 0.629 (0.053) |
| **aBMD femur ($g.cm^{-2}$)** | 0.783 (0.098) | 0.737 (0.084)* | 0.707 (0.095)*** | 0.747 (0.083) | 0.764 (0.064) |
| **aBMD spine ($g.cm^{-2}$)** | 0.848 (0.181) | 0.833 (0.144) | 0.869 (0.097) | 0.804 (0.142) | 0.878 (0.172) |

aBMD neck was lower in fractured groups (all $p < 0.05$), except in the WF group ($p > 0.05$). The F and HF groups were associated with lower aBMD femur ($p < 0.05$). aBMD spine was not different between fractured and non-fractured groups. Ct.ThUS was consistently lower in fractured groups (2.61-2.87 mm; all $p < 0.05$), except in the WF group (2.91 mm; $p > 0.05$) in comparison with the non-fractured group (3.02 mm). Ct.PoUS was higher in all fractured groups (11.6-12.8%; all $p < 0.001$), except in the HF group (9.4%; $p > 0.05$) compared to the non-fractured group (10.2%). Note that a lower height was observed in the F and VF groups ($p < 0.05$) while no difference existed in BMI and weight between groups.

*Spearman's rank correlation analysis*

The correlation results are summarized in Table 2. aBMD femur, aBMD neck and aBMD spine were all correlated (R from 0.46 to 0.84; all $p < 0.001$). There was no correlation between $Ct.Th_{US}$ and $Ct.Po_{US}$. Weak correlations were observed between QUS and DXA results (R around 0.20; $p < 0.01$). $Ct.Th_{US}$ was not correlated with aBMD spine, whereas a weak correlation was observed for $Ct.Po_{US}$ ($R = 0.16$; $p < 0.05$). All QUS and DXA variables were correlated with age and BMI. The correlation of $Ct.Th_{US}$ to age is negative, while it is positive for $Ct.Po_{US}$. Age and BMI were not correlated.

*Table 2: Spearman's correlation coefficients R between US variables, aBMD, age and BMI (*p < 0.05, **p < 0.01, ***p < 0.001).*

| | $Ct.Th_{US}$ | $Ct.Po_{US}$ | aBMD neck | aBMD femur | aBMD spine | Age | BMI |
|---|---|---|---|---|---|---|---|
| **$Ct.Th_{US}$** | - | -0.01 | 0.23** | 0.19** | 0.07 | -0.35*** | 0.29*** |
| **$Ct.Po_{US}$** | -0.01 | - | -0.15* | -0.12 | -0.16* | 0.16* | -0.27*** |
| **aBMD neck** | 0.23** | -0.15* | - | 0.84*** | 0.46*** | -0.44*** | 0.33*** |
| **aBMD femur** | 0.19** | -0.12 | 0.84*** | - | 0.56*** | -0.40*** | 0.36*** |
| **aBMD spine** | 0.07 | -0.16* | 0.46*** | 0.56*** | - | -0.21*** | 0.3*** |
| **Age** | -0.35*** | 0.16* | -0.44*** | -0.40*** | -0.21*** | - | 0.00 |
| **BMI** | 0.29*** | -0.27*** | 0.33*** | 0.36*** | 0.3*** | 0.00 | - |

*Fracture discrimination*

Systematic adjustment for age, BMI and glucocorticoid treatment was made for all the analyses. The results of the logistic regression analysis and AUCs are shown in Table 3. Results for the adjusted variables are as follows. aBMD neck was discriminant for all non-traumatic fractures combined (AUC: 0.72; OR: 1.48) and marginally discriminant for hip fractures ($p = 0.063$). aBMD femur was discriminant for hip fracture only (AUC = 0.70; OR = 2.21). Lumbar spine aBMD was not discriminant for any fractured group. VF and WF groups could not be discriminated with any aBMD variable.

*Table 3: Odds ratios (ORs) and areas under the ROC curve (AUCs) (Reference category is NF (N=109). CI confidence interval. ROC receiver operating characteristic. AUCs and ORs are adjusted for age, BMI and glucorticoid treatment. The p values of significant results are indicated in bold: *p < 0.05, **p < 0.01, ***p < 0.001).*

With the exception of the HF group, $Ct.Po_{US}$ could discriminate all fractured groups from the non-fractured group (AUCs: 0.71-0.84; ORs: 1.39-1.96), whereas $Ct.Th_{US}$ was discriminant for hip fractures only (AUC: 0.72; OR: 2.01). For all non-traumatic fractures combined and hip fractures, aBMD neck performed slightly better than QUS parameters in terms of AUCs and ORs. For vertebral and wrist fractures, $Ct.Po_{US}$ was the only significant discriminator, with AUCs equal to 0.84 (VF) and 0.71 (WF) and ORs equal to 1.96 (VF) and 1.80 (WF), respectively. The magnitude of changes reached with a combination of QUS variables or a combination of QUS and aBMD variables was limited. $Ct.Po_{US}$ was found to be associated with all non-traumatic fractures combined independently from aBMD neck, while $Ct.Th_{US}$ was found to be associated with hip fracture independently from aBMD femur. Apart from the combination of aBMD femur and $Ct.Th_{US}$ weakly improving AUC from 0.72 to 0.74 (albeit nonsignificant) in case of hip fractures, there was no improvement in fracture risk prediction when combining different variables.

## DISCUSSION

This pilot study investigated the ability of two QUS cortical parameters, Ct.Th and Ct.Po, estimated from measurements at the one-third distal radius using a custom-made guided wave technology to discriminate postmenopausal women with non-traumatic fractures from the control group. The main findings from this study were that (i) Ct.Po was discriminant for all non-traumatic fractures combined and, in particular, for vertebral and wrist fractures, while Ct.Th was discriminant for hip fractures only; (ii) the demonstration of a significant association between increased porosity at the one-third distal radius assessed by BDAT and vertebral and wrist fractures when these fractures were not associated with any measured aBMD variables; (iii) the association between increased cortical porosity and all non-traumatic fractures

combined independently of aBMD neck; and (iv) the association between decreased cortical thickness and hip fractures independently of aBMD femur.

To the best of our knowledge, this study reports for the first time on the concurrent *in vivo* estimates of two cortical bone quality markers, *i.e.*, cortical thickness and porosity, using an ultrasound modality based on the propagation of guided waves, and their association with fractures. Some earlier studies have reported on fracture discrimination with ultrasound AT measurements at high (~1.0 MHz) or low frequencies (~250 kHz) on the radius or tibia.[21,22,24,48-50] Unlike these earlier studies relying on the FAS velocity, the estimated QUS parameters were here not directly measured but derived from a model-based inverse problem approach that was previously validated. This procedure, applied *in vivo* at the one-third distal radius of healthy subjects, yielded thickness estimates in good agreement with ground truth values derived from site-matched HR-pQCT measurements.[41] In addition, both Ct.Th and Ct.Po have been recently validated against traditional $\mu$-CT on *ex vivo* bone specimens.[40] Our Ct.Th values ranging from 1.6 to 3.9 mm are consistent with values obtained *in vivo* at the same site, *i.e.*, the one-third distal radius, using pulse-echo[51,52] or pQCT.[49] However, as no *in vivo* porosity measurement using QUS have been reported so far, our Ct.Po values, ranging from 3 to 21%, can only be compared with *ex vivo* reference values, obtained at the same site using synchrotron $\mu$-CT[53] or scanning acoustic microscopy.[54] It is also worth mentioning that ultrasound waves are elastic waves, which are sensitive to the effective elastic properties of the propagation medium. The effective elastic properties, *i.e.*, the homogenized elastic properties at the mm length scale, are partly determined by the microstructure. Therefore, in principle, our Ct.Po estimates reflect the porosity below the resolution limit of HR-pQCT.

QUS parameters could not be identified for 49 patients, and the failure rate (around 20%) was typically associated with higher BMI, as it was already evidenced in earlier studies relying on the FAS velocity.[23,48] Higher BMI implies a thicker soft tissue layer on top of bone, which complicates probe alignment with the main bone axis, entails higher signal attenuation and generates the presence of unwanted additional guided modes propagating in the soft tissue layer. Identification of cortical bone properties in presence of thick soft tissue may be challenging and may require more sophisticated models than the one used here.[55] The general complexity of cortical bone structure, and particularly the disruption of the endosteal bone edge and the presence of large resorption cavities that can be observed in case of strongly deteriorated bones,[56] may impact the generation and propagation of guided waves.[40] However, in this study the failure rate was not correlated with fracture history.

With the renewed interest in assessing *in vivo* the cortical compartment,[56] which has long been neglected, new techniques that measure critical indices beyond aBMD directly related to fracture risk such as cortical porosity and thickness have flourished in recent years. So far, the current gold standard for cortical micro-architecture assessment at the radius is HR-pQCT, which also provides estimates of Ct.Th and Ct.Po.[10] However, HR-pQCT is limited to clinical research facilities and will unlikely be used as a widespread diagnostic tool for osteoporosis due to cost issues and ionizing radiations. With the advantage of non- invasiveness and affordability, compact ultrasound devices that measure forearm (radius) or leg (tibia) cortical bone is a vivid research area.[16,41,49,51,57]

Central DXA measurements, performed at the lumbar spine, femoral neck and total femur, delivered reference aBMD values that serve as the gold standard for skeletal status assessment. At the vertebral site, aBMD values could not discriminate between controls and fractured subjects. This may be due to the small number ($n = 32$) of vertebral fractures. At the

femoral site, aBMD neck and aBMD femur differed between controls and all non-traumatic fractures combined, however aBMD neck was the only parameter able to discriminate hip fractures from controls, which may be an effect of the small sample size. Similar results have been reported in other cohort population studies.[58]

First, our results showed that Ct.Th and Ct.Po, as depicted by BDAT, exhibited significant age-related dependence for females: concurrent to the increased porosity, the thickness at the radius was reduced with aging. These results are consistent with data obtained previously with HR-pQCT.[10,56,59-63] Second, Ct.Th and Ct.Po were associated with fracture. There are no equivalent studies comparable to ours; however, many cross-sectional and retrospective studies have evaluated the association of HR-pQCT-derived cortical structural variables, Ct.Th and Ct.Po, measured at the ultradistal radius, with odds of prior fracture in women. These studies have demonstrated that alterations of cortical bone structure at the ultradistal radius, such as low Ct.Th[58,64-71] or high Ct.Po,[72,73] are associated with prevalent fracture. In a few studies, the association between Ct.Th and the existence of fractures remained significant even after adjustment for aBMD.[64,69]

All these previous studies rely on HR-pQCT, but only a few reports rely on the measurement of cortical thickness with QUS modalities. Mishima *et al.*[57] reported that Ct.Th measured in ultrasound transmission at the ultradistal radius was a significant factor independently associated with vertebral fractures in type 2 diabetes mellitus patients with low estimated glomerular filtration rate. The ability of Ct.Th measured at the radius or tibia with pulse-echo ultrasonometry and combined with patient characteristics (age, weight, and height) to discriminate postmenopausal patients with osteoporosis from those without osteoporosis (as measured by DXA of the hip) was reported by Schousboe *et al.*[52] In the same study, a significant association of tibial (but not radial) Ct.Th with all types of prior fractures was found.

In our study, guided waves measurements presented adjusted ORs and AUCs of comparable magnitude to aBMD measurements for all non-traumatic fractures combined and hip fractures. Interestingly, Ct.Th and Ct.Po were associated with fractures of different groups (Ct.Th for the HF group and Ct.Po for the VF and WF groups), suggesting the capability of QUS-based estimates of cortical bone structure characteristics to predict site-specific fracture risk. Furthermore, Ct.Po could discriminate the vertebral and wrist fractured groups from controls, when these two groups could not be discriminated using aBMD and an association between Ct.Po and all non-traumatic fractures combined, as well as between Ct.Th and hip fractures, independent of aBMD was observed. However, whether a combination of variables, ultrasonic or densitometric, could yield a better discrimination in comparison to a variable alone could not be demonstrated here. Our results confirm previous studies that showed alterations of cortical bone structure in subjects with fracture, and that these alterations are associated with hip, vertebral, wrist or all type of fragility fractures. However, altogether, the results of these studies and those of our study do not all concur on the discriminating ability of cortical thickness or porosity measured at the radius for different fracture skeletal sites and on the aBMD-independent association of these parameters after adjustment on the aBMD. Likely source of these discrepancies is the limited number of fractures in most studies. Furthermore, the region investigated with HR-pQCT is more distal than the one investigated with QUS, which calls for caution for the comparison of HR-pQCT and AT studies. To the best of our knowledge, there is only one report showing the ability of cortical thickness measured at the one-third distal radius (using pQCT) to retrospectively discriminate postmenopausal subjects with all types of low- or moderate-energy fracture from non-fractured subjects, with OR=1.51 and AUC=0.78 similar to ours.[49]

Our study had several limitations. A first limitation is the overall small number of patients and particularly the small number of fractures in each group. This pilot study with 20 to 30 fractured women in each fracture group may have been underpowered to provide robust estimates. Larger studies are needed to address the question of whether cortical thickness and porosity can be used as site-specific fracture risk factors and whether these parameters are risk indicators of fracture independent of aBMD, particularly in patients with normal aBMD, or if it offers additional discriminatory capacity over aBMD in a particular category of patients. In that vein, it would also be valuable to account for the number of vertebral fractures and fracture severity in the analysis. Nonetheless, such approach was not conducted here, because of the low sample sizes of the different sub-groups. A second limitation is that in absence of DXA measurements at the distal radius, we could not test whether, after adjusting for radial aBMD, differences between women with fracture and controls remained significant for the QUS variables, in particular for wrist fractures. Third, for sake of comparison with previous scans, our center continues analyzing only L2 to L4 vertebrae. However, to be consistent with most studies, analyzing L1 to L4 vertrebrae could lead to improved fracture discrimination of the VF group. This has to be taken into account in further studies. Fourth, BDAT measurements were done retrospectively after the fractures were sustained. The independent contribution of cortical structure as depicted by ultrasound to the risk of fracture has to be evaluated prospectively. Fifth, the free plate model used for cortical bone characteristics identification was parametrized in terms of thickness and porosity, assuming universal material properties of the tissue matrix. Fixed matrix properties did not take into account the inevitable inter-individual variability of bone tissue properties.[74] However, such a hypothesis has been found to yield reasonably accurate *ex vivo* identification of Ct.Th and Ct.Po of human radius and tibia specimens.[40] This model simplification can be avoided using a model parametrized in terms of thickness and stiffness (*i.e.*, including four independent stiffness coefficients to account for the generally accepted transverse isotropy of cortical long bones measured axially). Our group achieved concurrent estimates of both thickness and bulk wave velocities (directly reflecting the elastic properties) of cortical bone using such a transverse isotropic plate model.[37,55] However, as experimental dispersion curves are usually incomplete and noisy, solving such a multiparametric inverse problem could lead to an ill-posed inversion (*i.e.*, numerous local optima) and overfitting of the data. To make this technique available in clinical studies, simplifications of the model are currently required to reduce computing time and ensure robustness of parameters identification. An important current limitation of our BDAT approach is that it fails when the thickness of soft tissue is large (*i.e.*, typically associated with BMI larger than 28 $kg.m^{-2}$ in this study). Further research is warranted to make this technology available to patients with BMI above 28 $kg.m^{-2}$. The focus will be on the improvement of the HMI (by including quantitative features delivering a real time feedback on the probe alignment) and on the development of more sophisticated waveguide models accounting for the soft tissue layer (whose thickness could be evaluated by conventional pulse-echo imaging for instance). Finally, the prototype status of the device should be considered when interpreting the results. The role of the operator in data acquisition is critical. At this stage, the operator ability to correctly align the probe along the main bone axis is a key issue for the measurement success. The measurement protocol has been carefully designed to guide the operator and optimize the measurement reproducibility, but it is expected that ongoing developments of the probe, the HMI and the methodology may lead to improved fracture discrimination in the future. Reproducibility studies on patients are currently being conducted in different healthcare centers with an updated version of the HMI.

## CONCLUSION

In summary, our results indicate that BDAT measurements at the one-third distal radius may be used to characterize cortical bone in postmenopausal women. Ct.Po was discriminant for all non-traumatic fractures combined and, in particular, vertebral and wrist fractures when these fractures were not associated with any measured aBMD variables, while Ct.Th was discriminant for hip fractures only. These results open perspectives to the clinical assessment of cortical bone using a portable and non-ionizing device.

## ACKNOWLEDGMENT

This work received financial support from the Fondation pour la Recherche Médicale (FRM DBS201311228444), MSD and Azalée.

Authors' roles: Study design: PL and CR. Patient recruitment: SK, KB, and CR. US reproducibility study: DR and JGM. US data collection: QV, NB, and JGM. Data analysis: DR and JGM. Drafting manuscript: JGM and DR. Revising manuscript content: All authors. AE and JGM take responsibility for the integrity of the data analysis.

## REFERENCES

1. Seeman E, Delmas P. Bone quality - the material and structural basis of bone strength and fragility. N Engl J Med. 2006; 354(21):2250-2261.
2. Curtis E, Moon R, Harvey N, Cooper C. The impact of fragility fracture and approaches to osteoporosis risk assessment worldwide. Bone. 2017; 104:29-38.
3. Haentjens P, Magaziner J, Colon-Emeric C, Vanderschueren D, Milisen K, Velkeniers B, et al. Meta-analysis: excess mortality after hip fracture among older women and men. Ann Intern Med. 2010; 152(6):380-390.
4. Van Den Bergh J, Van Geel T, Geusens P. Osteoporosis, frailty and fracture: implications for case finding and therapy. Nat Rev Rheumatol. 2012; 8(3):163.
5. Kanis J, Johnell O, Oden A, Dawson A, De Laet C, Jonsson B. Ten year probabilities of osteoporotic fractures according to BMD and diagnostic thresholds. Osteoporos Int. 2001; 12(12):989-995.
6. Siris E, Chen YT, Abbott T, Barrett-Connor E, Miller P, Wehren L, et al. Bone mineral density thresholds for pharmacological intervention to prevent fractures. Arch Intern Med. 2004; 164(10):1108-1112.
7. Geusens P, Van Geel T, Huntjens K, Van Helden S, Bours S, Van Den Bergh J. Clinical fractures beyond low BMD. Int J Clin Rheumtol. 2011;6(4):411.
8. Lespessailles E, Cortet B, Legrand E, Guggenbuhl P, Roux C. Low-trauma fractures without osteoporosis. Osteoporos Int. 2017; 28(6):1771-1778.
9. Shigdel R, Osima M, Ahmed L, Joakimsen R, Eriksen E, Zebaze R, et al. Bone turnover markers are associated with higher cortical porosity, thinner cortices, and larger size of the proximal femur and non-vertebral fractures. Bone. 2015; 81:1-6.
10. Nishiyama K, Macdonald H, Buie H, Hanley D, Boyd S. Postmenopausal women with osteopenia have higher cortical porosity and thinner cortices at the distal radius and tibia than women with normal aBMD: an in vivo HR-pQCT study. J Bone Miner Res. 2010; 25(4):882-890.

11. Augat P, Schorlemmer S. The role of cortical bone and its microstructure in bonestrength. Age Ageing. 2006; 35(suppl 2):ii27-ii31.

12. Bala Y, Zebaze R, Seeman E. Role of cortical bone in bone fragility. Curr Opin Rheumatol. 2015; 27(4):406-413.

13. Cooper D, Kawalilak C, Harrison K, Johnston B, Johnston J. Cortical Bone Porosity: What Is It, Why Is It Important, and How Can We Detect It? Curr Osteoporos Rep. 2016; 14(5):187-198.

14. Zebaze R, Ghasem-Zadeh A, Mbala A, Seeman E. A new method of segmentation of compact-appearing, transitional and trabecular compartments and quantification of cortical porosity from high resolution peripheral quantitative computed tomographic images. Bone. 2013; 54(1):8-20.

15. Diez-Perez A, Güerri R, Nogues X, Cáceres E, Peña M, Mellibovsky L, et al. Microindentation for in vivo measurement of bone tissue mechanical properties in humans. J Bone Miner Res. 2010; 25(8):1877-1885.

16. Stein E, Rosete F, Young P, Kamanda-Kosseh M, McMahon D, Luo G, et al. Clinical assessment of the 1/3 radius using a new desktop ultrasonic bone densitometer. Ultrasound Med Biol. 2013; 39(3):388-395.

17. Sai H, Iguchi G, Tobimatsu T, Takahashi K, Otani T, Horii K, et al. Novel ultrasonic bone densitometry based on two longitudinal waves: significant correlation with pQCT measurement values and age-related changes in trabecular bone density, cortical thickness, and elastic modulus of trabecular bone in a normal Japanese population. Osteoporos Int. 2010; 21(10):1781-1790.

18. Mano I, Horii K, Hagino H, Miki T, Matsukawa M, Otani T. Estimation of in vivo cortical bone thickness using ultrasonic waves. J Med Ultrason. 2015; 42(3):315-322.

19. Talmant M, Foiret J, Minonzio JG. Guided waves in cortical bone. In: Bone quantitative ultrasound. Springer; 2011. p. 147-179.

20. Hans D, Baim S. Quantitative Ultrasound (QUS) in the management of osteoporosis and assessment of fracture risk. J Clin Densitom. 2017; 20(3):322-333.

21. Foldes A, Rimon A, Keinan D, Popovtzer M. Quantitative ultrasound of the tibia: a novel approach for assessment of bone status. Bone. 1995; 17(4):363-367.

22. Barkmann R, Kantorovich E, Singal C, Hans D, Genant H, Heller M, et al. A new method for quantitative ultrasound measurements at multiple skeletal sites: first results of precision and fracture discrimination. J Clin Densitom. 2000; 3(1):1-7.

23. Weiss M, Ben-Shlomo A, Hagag P, Rapoport M. Reference database for bone speed of sound measurement by a novel quantitative multi-site ultrasound device. Osteoporos Int. 2000; 11(8):688-696.

24. Knapp K, Blake G, Spector T, Fogelman I. Multisite quantitative ultrasound: precision, age-and menopause-related changes, fracture discrimination, and T-score equivalence with dual-energy X-ray absorptiometry. Osteoporos Int. 2001; 12(6):456-464.

25. Olszynski W, Brown J, Adachi J, Hanley D, Ioannidis G, Davison K, et al. Multisite quantitative ultrasound for the prediction of fractures over 5 years of follow-up: The Canadian Multicentre Osteoporosis Study. J Bone Miner Res. 2013; 28(9):2027-2034.

26. Nicholson P, Moilanen P, Kärkkäinen T, Timonen J, Cheng S. Guided ultrasonic waves in long bones: modelling, experiment and in vivo application. Physiol Meas. 2002; 23(4):755.

27. Moilanen P. Ultrasonic guided waves in bone. IEEE Trans Ultrason Ferroelectr Freq Control. 2008; 55(6):1277 - 1286.

28. Moilanen P, Nicholson P, Kilappa V, Cheng S, Timonen J. Assessment of the cortical bone thickness using ultrasonic guided waves: Modelling and in vitro study. Ultrasound Med Biol. 2007; 33(2):254-262.

29. Minonzio JG, Talmant M, Laugier P. Guided wave phase velocity measurement using multi-emitter and multi-receiver arrays in the axial transmission configuration. J Acoust Soc Am. 2010; 127(5):2913-2919.

30. Tran T, Nguyen KC, Sacchi M, Le L. Imaging ultrasonic dispersive guided wave energy in long bones using linear radon transform. Ultrasound Med Biol. 2014; 40(11):2715-2727.

31. Xu K, Ta D, Cassereau D, Hu B, Wang W, Laugier P, et al. Multichannel processing for dispersion curves extraction of ultrasonic axial-transmission signals: Comparisons and case studies. J Acoust Soc Am. 2016; 140(3):1758-1770.

32. Okumura S, Nguyen VH, Taki H, Haïat G, Naili S, Sato T. Rapid high-resolution wavenumber extraction from ultrasonic guided waves using adaptive array signal processing. Appl Sci. 2018; 8(4):652.

33. Moilanen P, Talmant M, Kilappa V, Nicholson P, Cheng S, Timonen J, et al. Modeling the impact of soft tissue on axial transmission measurements of ultrasonic guided waves in human radius. J Acoust Soc Am. 2008; 124(4):2364-2373.

34. Ta D, Wang W, Wang Y, Le L, Zhou Y. Measurement of the dispersion and attenuation of cylindrical ultrasonic guided waves in long bone. Ultrasound Med Biol. 2009; 35(4):641-652.

35. Nguyen VH, Tran T, Sacchi M, Naili S, Le L. Computing dispersion curves of elastic / viscoelastic transversely-isotropic bone plates coupled with soft tissue and marrow using semi-analytical finite element (SAFE) method. Comput Biol Med. 2017; 87:371-381.

36. Lefebvre F, Deblock Y, Campistron P, Ahite D, Fabre J. Development of a new ultrasonic technique for bone and biomaterials in vitro characterization. J Biomed Mater Res A. 2002; 63(4):441-446.

37. Foiret J, Minonzio JG, Chappard C, Talmant M, Laugier P. Combined estimation of thickness and velocities using ultrasound guided waves: A pioneering study on in vitro cortical bone samples. IEEE Trans Ultrason Ferroelect Freq Control. 2014; 61(9):1478-1488.

38. Bochud N, Vallet Q, Bala Y, Follet H, Minonzio J, Laugier P. Genetic algorithms-based inversion of multimode guided waves for cortical bone characterization. Phys Med Biol. 2016; 61(19):6953.

39. Bossy E, Talmant M, Defontaine M, Patat F, Laugier P. Bidirectional axial transmission can improve accuracy and precision of ultrasonic velocity measurement in cortical bone: A validation on test materials. IEEE Trans Ultrason Ferroelect Freq Control. 2004; 51(1):71-79.

40. Minonzio JG, Bochud N, Vallet Q, Bala Y, Ramiandrisoa D, Follet H, et al. Bone cortical thickness and porosity assessment using ultrasound guided waves: An ex vivo validation study. Bone. 2018; 116:111-119.

41. Vallet Q, Bochud N, Chappard C, Laugier P, Minonzio JG. In vivo characterization of cortical bone using guided waves measured by axial transmission. IEEE Trans Ultrason Ferroelect Freq Control. 2016; 63(9):1361-1371.

42. Warriner A, Patkar N, Curtis J, Delzell E, Gary L, Kilgore M, et al. Which fractures are most attributable to osteoporosis? J Clin Epidemiol. 2011; 64(1):46-53.

43. Moreau L, Minonzio JG, Foiret J, Bossy E, Talmant M, Laugier P. Accurate measurement of guided modes in a plate using a bidirectional approach. J Acoust Soc Am. 2014; 135(1):EL15-EL21.

44. Minonzio JG, Foiret J, Talmant M, Laugier P. Impact of attenuation on guided mode wavenumber measurement in axial transmission on bone mimicking plates. J Acoust Soc Am. 2011; 130(6):3574-3582.

45. Granke M, Grimal Q, Saïeed A, Nauleau P, Peyrin F, Laugier P. Change in porosity is the major determinant of the variation of cortical bone elasticity at the millimeter scale in aged women. Bone. 2011; 49(5):1020-1026.

46. Parnell W, Vu M, Grimal Q, Naili S. Analytical methods to determine the e_ective mesoscopic and macroscopic elastic properties of cortical bone. Biomech Model Mechanobiol. 2012; 11(6):883-901.

47. Orgee J, Foster H, McCloskey E, Khan S, Coombes G, Kanis J. A precise method for the assessment of tibial ultrasound velocity. Osteoporos Int. 1996; 6(1):1-7.

48. Talmant M, Kolta S, Roux C, Haguenauer D, Vedel I, Cassou B, et al. In vivo performance evaluation of bi-directional ultrasonic axial transmission for cortical bone assessment. Ultrasound Med Biol. 2009; 35(6):912-919.

49. Moilanen P, Määttä M, Kilappa V, Xu L, Nicholson P, Alén M, et al. Discrimination of fractures by low-frequency axial transmission ultrasound in postmenopausal females. Osteoporos Int. 2013; 24(2):723-730.

50. Määttä M, Moilanen P, Timonen J, Pulkkinen P, Korpelainen R, Jämsä T. Association between low-frequency ultrasound and hip fractures-comparison with DXA-based BMD. BMC Musculoskelet Disord. 2014; 15(1):208.

51. Karjalainen J, Riekkinen O, Töyräs J, Jurvelin J, Kröger H. New method for point-ofcare osteoporosis screening and diagnostics. Osteoporos Int. 2016; 27(3):971-977.

52. Schousboe J, Riekkinen O, Karjalainen J. Prediction of hip osteoporosis by DXA using a novel pulse-echo ultrasound device. Osteoporos Int. 2017; 28(1):85-93.

53. Bossy E, Talmant M, Peyrin F, Akrout L, Cloetens P, Laugier P. An in vitro study of the ultrasonic axial transmission technique at the radius: 1-MHz velocity measurements are sensitive to both mineralization and intracortical porosity. J Bone Miner Res. 2004; 19(9):1548-1556.

54. Raum K, Leguerney I, Chandelier F, Bossy E, Talmant M, Saïed A, et al. Bone microstructure and elastic tissue properties are reflected in QUS axial transmission measurements. Ultrasound Med Biol. 2005; 31(9):1225-1235.

55. Bochud N, Vallet Q, Minonzio JG, Laugier P. Predicting bone strength with ultrasonic guided waves. Sci Rep. 2017; 7:43628.

56. Zebaze R, Ghasem-Zadeh A, Bohte A, Iuliano-Burns S, Mirams M, Price R, et al. Intracortical remodelling and porosity in the distal radius and post-mortem femurs of women: a cross-sectional study. The Lancet. 2010; 375(9727):1729-1736.

57. Mishima T, Motoyama K, Imanishi Y, Hamamoto K, Nagata Y, Yamada S, et al. Decreased cortical thickness, as estimated by a newly developed ultrasound device, as a risk for vertebral fracture in type 2 diabetes mellitus patients with eGFR of less than 60 mL/min/1.73 m2. Osteoporos Int. 2015; 26(1):229-236.

58. Vico L, Zouch M, Amirouche A, Fr_ere D, Laroche N, Koller B, et al. High-resolution pQCT analysis at the distal radius and tibia discriminates patients with recent wrist and femoral neck fractures. J Bone Miner Res. 2008; 23(11):1741-1750.

59. Nicks K, Amin S, Atkinson E, Riggs B, Melton L, Khosla S. Relationship of age to bone microstructure independent of areal bone mineral density. J Bone Miner Res. 2012; 27(3):637-644.

60. Bala Y, Zebaze R, Ghasem-Zadeh A, Atkinson E, Iuliano S, Peterson J, et al. Cortical porosity identifies women with osteopenia at increased risk for forearm fractures. J Bone Miner Res. 2014; 29(6):1356-1362.

61. Shanbhogue V, Brixen K, Hansen S. Age-and sex-related changes in bone microarchitecture and estimated strength: a three-year prospective study using HRpQCT. J Bone Miner Res. 2016; 31(8):1541-1549.

62. Vilayphiou N, Boutroy S, Sornay-Rendu E, Van Rietbergen B, Chapurlat R. Age-related changes in bone strength from HR-pQCT derived microarchitectural parameters with an emphasis on the role of cortical porosity. Bone. 2016; 83:233-240.

63. Alvarenga J, Fuller H, Pasoto S, Pereira R. Age-related reference curves of volumetric bone density, structure, and biomechanical parameters adjusted for weight and height in a population of healthy women: an HR-pQCT study. Osteoporos Int. 2017; 28(4):1335-1346.

64. Boutroy S, Khosla S, Sornay-Rendu E, Zanchetta M, McMahon D, Zhang C, et al. Microarchitecture and peripheral BMD are impaired in postmenopausal white women with fracture independently of total hip T-score: an international multicenter study. J Bone Miner Res. 2016; 31(6):1158-1166.

65. Boutroy S, Van Rietbergen B, Sornay-Rendu E, Munoz F, Bouxsein M, Delmas P. Finite element analysis based on in vivo HR-pQCT images of the distal radius is associated with wrist fracture in postmenopausal women. J Bone Miner Res. 2008; 23(3):392-399.

66. Nishiyama K, Macdonald H, Hanley D, Boyd S. Women with previous fragility fractures can be classified based on bone microarchitecture and finite element analysis measured with HR-pQCT. Osteoporos Int. 2013;24(5):1733-1740.

67. Melton L, Christen D, Riggs B, Achenbach S, Müller R, van Lenthe G, et al. Assessing forearm fracture risk in postmenopausal women. Osteoporos Int. 2010; 21(7):1161-1169.

68. Zhu T, Hung V, Cheung WH, Cheng J, Qin L, Leung KS. Value of Measuring Bone Microarchitecture in Fracture Discrimination in Older Women with Recent Hip Fracture: A Case-control Study with HR-pQCT. Sci Rep. 2016; 6:34185.

69. Sornay-Rendu E, Cabrera-Bravo JL, Boutroy S, Munoz F, Delmas P. Severity of vertebral fractures is associated with alterations of cortical architecture in postmenopausal women. J Bone Miner Res. 2009; 24(4):737-743.

70. Wang J, Stein E, Zhou B, Nishiyama K, Yu Y, Shane E, et al. Deterioration of trabecular plate-rod and cortical microarchitecture and reduced bone stiffness at distal radius and tibia in postmenopausal women with vertebral fractures. Bone. 2016; 88:39-46.

71. Sornay-Rendu E, Boutroy S, Duboeuf F, Chapurlat R. Bone microarchitecture assessed by HR-pQCT as predictor of fracture risk in postmenopausal women: the OFELY study. J Bone Miner Res. 2017; 32(6):1243-1251.

72. Bala Y, Bui Q, Wang XF, Iuliano S, Wang Q, Ghasem-Zadeh A, et al. Trabecular and cortical microstructure and fragility of the distal radius in women. J Bone Miner Res. 2015; 30(4):621-629.

73. Edwards M, Robinson D, Ward K, Javaid M, Walker-Bone K, Cooper C, et al. Cluster analysis of bone microarchitecture from high resolution peripheral quantitative computed tomography demonstrates two separate phenotypes associated with high fracture risk in men and women. Bone. 2016; 88:131-137.

74. Unal M, Creecy A, Nyman J. The Role of Matrix Composition in the Mechanical Behavior of Bone. Curr Osteoporos Rep. 2018; 16(3):205-215.

# Ultrasound-based estimates of cortical bone thickness and porosity are associated with non-traumatic fractures in postmenopausal women: A pilot study

J.-G. Minonzio[1,*], N. Bochud[1], Q. Vallet[1], D. Ramiandrisoa[1], A. Etcheto[2], K. Briot[2,3], S. Kolta[2,3], C. Roux[2,3,4] and P. Laugier[1]

[1]*Sorbonne Université, CNRS, INSERM, Laboratoire d'Imagerie Biomédicale, F-75006, Paris, France*

[2]*INSERM UMR-1153, Paris, France*

[3]*Department of Rheumatology, Cochin Hospital, Assistance Publique–Hôpitaux de Paris, Paris, France*

[4]*Paris-Descartes University, Paris, France*

**Abstract**

Recent ultrasound axial transmission techniques exploit the multimode waveguide response of long bones to yield estimates of cortical bone structure characteristics. This pilot cross-sectional study aimed to evaluate the performance at the one-third distal radius of a bidirectional axial transmission (BDAT) device to discriminate between fractured and non-fractured postmenopausal women. Cortical thickness (Ct.Th) and porosity (Ct.Po) estimates were obtained for 201 postmenopausal women, among whom 109 were non-fractured (62.6±7.8 years), 92 with one or more non-traumatic fractures (68.8±9.2 years), 17 with hip fractures (66.1±10.3 years), 32 with vertebral fractures (72.4±7.9 years), and 17 with wrist fractures (67.8±9.6 years). The areal bone mineral density (aBMD) was obtained using dual-energy X-ray absorptiometry (DXA) at the femur and spine. Femoral aBMD correlated weakly but significantly with Ct.Th (R=0.23, $p < 0.001$) and Ct.Po (R=-0.15, $p < 0.05$). Femoral aBMD and both ultrasound parameters were significantly different between the subgroup of all non-traumatic fractures combined and the control group ($p < 0.05$). The main findings were (i) that Ct.Po was discriminant for all non-traumatic fractures combined (odds ratio OR=1.39; area under the receiver operating characteristic curve AUC=0.71), for vertebral (OR=1.96; AUC=0.84) and wrist fractures (OR=1.80; AUC=0.71), while Ct.Th was discriminant for hip fractures only (OR=2.01; AUC=0.72); (ii) the demonstration of a significant association between increased Ct.Po and vertebral and wrist fractures when these

fractures were not associated with any measured aBMD variables; (iii) the association between increased Ct.Po and all non-traumatic fractures combined independently of aBMD neck; and (iv) the association between decreased Ct.Th and hip fractures independently of aBMD femur. BDAT variables showed comparable performance to that of aBMD neck with all types of fractures (OR=1.48; AUC=0.72) and that of aBMD femur with hip fractures (OR=2.21; AUC=0.70). If these results are confirmed in prospective studies, cortical BDAT measurements may be considered useful for assessing fracture risk in postmenopausal women.
*Keywords:* Cortical bone; osteoporosis; fracture discrimination; quantitative ultrasound; guided waves

## 1. Introduction

Osteoporosis is a skeletal disease leading to bone fragility and increasing the risk of fractures.[1] Osteoporosis still remains a major public health problem worldwide[2] and it is therefore crucial to prevent severe fractures responsible for excess of mortality and considerable morbidity.[3,4] Patients are currently identified as having osteoporosis using dual-energy X-ray absorptiometry (DXA), assessing the areal bone mineral density (aBMD), directly measured at the main fracture sites, *i.e.*, hip and spine.[5] However, even though DXA remains the current gold standard, it is limited by the difficulty to set a threshold for fracture risk in the aBMD distribution.[6] Indeed, more than half of individuals who have low-trauma fractures have a T-score higher than the osteoporotic threshold defined by the World Health Organization (*i.e.*, T-score = -2.5).[7] Moreover, some diseases (diabetes, obesity) and treatments (glucocorticoids) are associated with an increase of fracture risk without an aBMD decrease.[8]

One of the reasons for the limitation of DXA is that it does not capture alterations of bone quality factors, namely the material and structural properties, and particularly those of cortical bone. Because of its projection technique, DXA is not able to separate the trabecular and cortical compartments. Impaired bone remodeling affects not only the trabecular compartment but also the cortical one, inducing thickness decrease and porosity increase.[9,10] Despite the crucial contribution of the cortical structure and microstructure to the whole bone mechanical competence, cortical bone was understudied for a long time.[11,12] Recent

advances in high resolution imaging technology have driven growing recognition of the role of cortical microstructure in osteoporotic bone loss and fragility.[13]

In the past two decades, there has been a great deal of interest in new techniques to assess cortical bone. The high resolution peripheral quantitative computed tomography (HR-pQCT) technique has seen recent developments with regard to the assessment of cortical porosity.[10,14] Reference point indentation is proposed to assess the mechanical behavior of cortical bone.[15] There are currently different approaches for quantitative ultrasound (QUS) based on mechanical waves propagation, which possess intrinsic sensitivity to bone elastic and structural properties: transverse transmission measuring cortical bone at the one-third radius,[16] transverse transmission based on two longitudinal waves at the ultradistal radius,[17] pulse-echo techniques,[18] and axial transmission (AT),[19] specifically designed to measure cortical bone. Unlike HR-pQCT and reference point indentation, QUS has the advantages of portability, low cost, non-invasiveness, absence of radiation and no need for a radiographic technologist or designated room.[20]

In AT, transducers (emitters and receivers) aligned along the main bone axis are used to measure the speed of sound of waves guided along the cortex of a long bone, such as the radius or tibia.[21] With earlier approaches, analyses of AT signals were restricted to a single waveform, either the first arriving signal (FAS) or the fundamental flexural guided wave (FFGW). FAS velocity measured at the radius demonstrated ability to discriminate fracture cases from controls in postmenopausal women in numerous clinical studies, although, compared to DXA, FAS velocity has not shown superiority for fracture prediction.[22–25] The identification of the FFGW,[26] a slower waveform than FAS, whose dispersion characteristics (frequency-related phase velocity variations) are sensitive to cortical thickness for frequency thickness product lower than 0.5 MHz.mm,[27] has been a positive turning point for ultrasound cortical bone assessment. Indeed, while the precise bone properties reflected by FAS remain to be established, the FFGW velocity can be predicted with analytical models and thus an inverse problem approach allows inferring cortical thickness from measurements.[28] For a given waveguide and frequency bandwidth, multiple guided modes can coexist. These multiple modes contain more information than a single mode. Thus, the earlier analysis of AT signals, so far limited to a single waveform, has been extended to a full-waveform analysis.

The problem is that, in the full waveform, distinguishing modes or their dispersion curves in recorded signals requires specific acquisition scheme or signal processing. Over the past years, the determination of guided modes and identification of cortical bone waveguide characteristics has sparked increased discussions of signal processing approaches,[29–32] modeling,[33–35] and inverse problem solving.[28,36–38]

Our group has developed the bidirectional axial transmission (BDAT) to this goal.[39] We recently showed that BDAT combined with an appropriate waveguide model allows the concurrent identification of cortical thickness and porosity of *ex vivo* human specimens.[40] In a pilot *in vivo* study, BDAT could identify cortical thickness nearly as accurately as conventional HR-pQCT.[41] Assessment of cortical thickness (Ct.Th) and porosity (Ct.Po) by BDAT may improve the identification of patients at high risk of fracture. Therefore, in this study, we compared *in vivo* measurements of spine and hip aBMD to cortical bone thickness and porosity assessed by BDAT in postmenopausal women with and without prior history of fracture. Our aim was to study whether these ultrasound parameters were associated with fracture.

## 2. Materials and Methods

*Subjects*

Three hundred and one patients were recruited from the Rheumatology Department in Cochin Hospital, Paris, France, between April 2014 and November 2015. All of them were ambulatory female patients consulting for fracture risk assessment. The study has been approved by the ethical committee of the Committees for the protection of persons Ile de France III. A written informed consent was provided by the patients. The procedure of the study was in accordance with the Declaration of Helsinki. The fracture information, including site and time, was collected in medical records; and the diagnosis of vertebral fractures was confirmed based on spine imaging. Fractures were classified as traumatic and non-traumatic.

Five groups were created: a control group with patients without fracture (NF); patients with any non-traumatic fracture (F); patients with a hip fracture (HF); patients with one or several vertebral fractures (VF) and patients with a wrist fracture (WF).[42] Note that the groups were classified as follows: the HF group contained at least a hip fracture and

potentially other fractures, the VF group did not contain hip fractures and likewise the WF group did not contain hip and vertebral fractures. Exclusion criteria were: missing data ($n = 7$), patient suffering from a cancer ($n = 1$), two-hip replacement (no femoral DXA possible, $n = 9$), BMI $< 15$ ($n = 1$), and a history of traumatic fractures ($n = 33$). Thus, 250 postmenopausal women are the basis of this cross-sectional study. Note that among the VF group, 16 patients only had one vertebral fracture, 11 had two vertebral fractures and 5 had more than two vertebral fractures. The number of patients undergoing glucocorticoid treatment was as follows: 12 in the NF group and 12 in the F group.

*Ultrasonic measuring device*

The QUS device (Azalée, Paris, France) consists of three custom-made parts [Fig. 1(a)]. First, a 1-MHz BDAT probe adapted to forearm measurements (Vermon, Tours, France), which is composed of a linear array of piezocomposite elements divided in one array of 24 receivers surrounded by two arrays of 5 transmitters each. The probe has been specifically designed to measure guided waves propagating in two opposite directions and thus correct the bias on the guided modes wavenumbers induced by the inclination angle between the probe and the bone due to uneven overlying soft tissues.[39,43] Second, an electronic device used to transmit, receive and digitize signals (Althaïs, Tours, France). The electronic device allows exciting each transmitter successively with a wideband pulse (170 V, 1-MHz central frequency) of -6 dB power spectrum spanning the frequency range from 0.4 to 1.6 MHz. The received signals are 16 times averaged and then sampled with a 20 MHz frequency (1024 time samples, 12 bits). Third, a human machine interface (HMI, Bleu Solid, Paris, France), developed to display the spectrum of guided waves in quasi real-time (at a frame rate up to 4 Hz) and to guide the operator in finding during measurement the optimal position of the probe with respect to the main bone axis.

*Signal processing and cortical parameter identification*

Identification of cortical parameters is achieved through an approach that is an extension of the signal processing applied to extract the experimental guided mode wavenumbers from the maxima of the so-called *Norm* function.[29,44] The processing steps of the ultrasonic signals have been extensively described in our previous works.[41,44] Briefly, a singular value

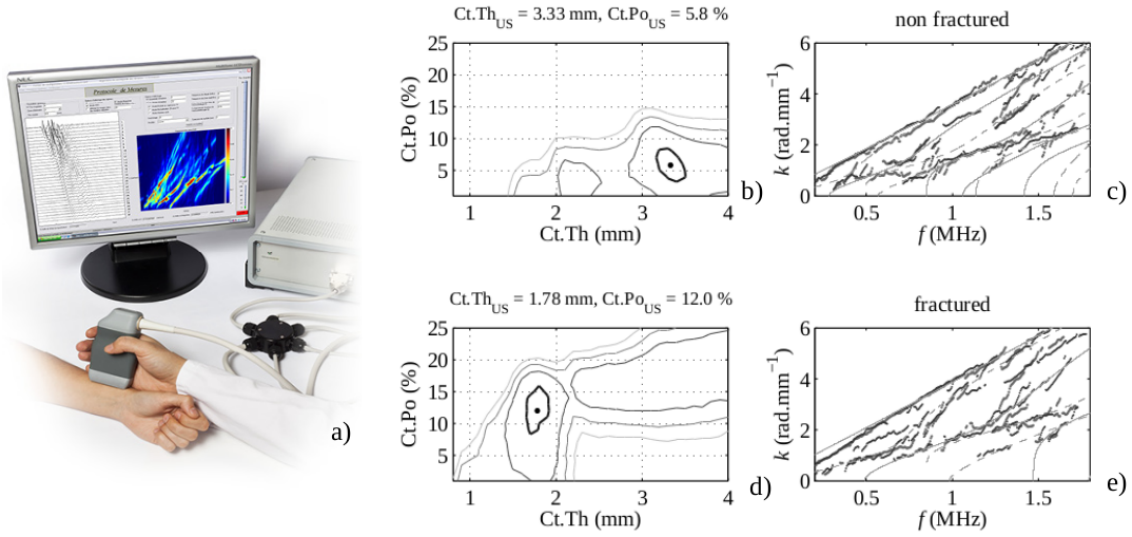


Figure 1: (a) Illustration of the BDAT prototype device placed at the lateral one-third distal radius; (b)-(c) Example of the projected function (Eq. (2)) and guided mode wavenumbers vs frequency for a non-fractured patient; (d)-(e) Example of the projected function (Eq. (2)) and guided mode wavenumbers vs frequency for a patient with a non-traumatic shoulder fracture. The maxima (black dot) of the projected functions shown in (b) and (d) corresponds to the optimal theoretical waveguide models, whose guided modes are shown in (c) and (e) with continuous lines. Experimental guided mode wavenumbers are shown with dots. Contours in (b) and (d) correspond to values equal to the maximum of the projected function minus 0.1, 0.2, 0.3 and 0.4. The area delimited by the highest (thick) line can be interpreted as the measurement resolution, *i.e.*, the ability of the measurement system to differentiate two close waveguide models. The resolution for the two ultrasound parameters is typically estimated to be about $\pm 0.2$ mm and $\pm 2$ %.

decomposition is applied at each frequency to the response matrix containing the temporal Fourier transforms of all transmitter-receiver signals. Signal-to-noise ratio enhancement is then achieved by retaining the singular vectors, denoted by $\boldsymbol{U}_n$, associated with the highest singular values, the lowest singular values being associated with noise. Finally, the projection of a variable testing vector onto the signal singular vector basis yields the *Norm* function. First, probe positioning is achieved by optimizing the *Norm* function, as it will be explained hereinafter in the measurement protocol section, which is defined as

$$Norm(f,k) \quad = \quad ||\boldsymbol{e}^{\text{test}}(k)||^2_{\boldsymbol{U}_n(f)} \; . \tag{1}$$

In this case, the testing vector $\boldsymbol{e}^{\text{test}}$ is a normalized attenuated plane wave.[44] This vector spans all waves measurable by the device corresponding to all frequencies $f$ and wavenumbers $k$ of the device bandwidth. Thus, each plane wave is associated with a pixel $(f,k)$ of the

*Norm* function, defined by the norm of the projected testing vector. The pixel value range reflects in a 0-1 scale the presence rate of the tested wave in the measured signals. The *Norm* function can thus be interpreted as an enhanced spatio-temporal Fourier transform.[29]

Second, in the case of waveguide parameters estimation, instead of spanning all measurable waves, the testing vectors are limited to the guided modes of a dedicated cortical bone waveguide model.[40] The waveguide model is a 2-D transverse isotropic free plate, parametrized in terms of thickness and elasticity.[37] Subsequently, we use an asymptotic homogenization approach to predict the mesoscopic stiffness coefficients from the microstructure, so that the elasticity of our model is parametrized in terms of porosity, assuming the bone matrix being spatially homogeneous and uniform among individuals.[45,46] The waveguide model corresponds to $M$ testing vectors depending on the guided mode wavenumbers, denoted by $k_m(f, Ct.Th, Ct.Po)$. Each pair of values (Ct.Th, Ct.Po) is associated with a projected value $Proj(Ct.Th, Ct.Po)$ defined by

$$Proj(Ct.Th, Ct.Po) = \frac{1}{f_{\max} - f_{\min}} \int_{f_{\min}}^{f_{\max}} \frac{1}{M} \sum_{m=1}^{M} \left|\left| \boldsymbol{e}^{\text{test}} \left(k_m(f, Ct.Th, Ct.Po)\right)\right|\right|^2_{\boldsymbol{U}_n(f)} df \quad (2)$$

where $f_{\min}$ and $f_{\max}$ are the frequency bandwidth limits. This equation corresponds to the weight of each testing vector for the whole frequency bandwidth. The highest magnitude of the projected function corresponds to the optimal pair of ultrasound parameters (denoted hereafter as $\text{Ct.Th}_{\text{US}}$ and $\text{Ct.Po}_{\text{US}}$) that allows reaching the best fit between the model and the experimental data. Representative examples of projected functions [Eq. (2)] are shown for a non-fractured [Fig. 1(b)] and a fractured [Fig. 1(d)] patient. The associated optimal waveguide model is shown in Figs. 1(c) and (e) together with the experimental guided modes obtained from the maxima of the *Norm* function [Eq. (1)].

*Measurement protocol*

A specific scanning methodology was carefully followed for measuring the patients. Measurements were done on the non-dominant forearm. When the non-dominant forearm undergoes a recent fracture, measurements were done on the contralateral arm. BDAT measurements were performed on a standardized region of interest (ROI), *i.e.*, the center of the probe was placed at the lateral side of the one-third distal radius (*i.e.*, 70 mm away from the

radial styloid). The ROI length corresponds to the length of the receiver array (about two centimeters; the whole probe length being about five centimeters). The probe was placed in contact with the skin using ultrasonic gel for coupling (Aquasonic, Parker Labs Inc., Fairfield NJ, USA).

The measurement protocol consists of multiple series of ten acquisitions. By means of a visual inspection of the spectrum of guided waves displayed in real time by the HMI, once a correct probe position is found, ten successive acquisitions are recorded without moving the probe. The visual inspection relies on the following criteria: (i) the dispersion spectrum contains at least 3–4 guided modes (in particular, the low-order antisymmetric mode and higher-order modes, which are highly sensitive to the porosity and thickness of the waveguide, respectively); (ii) the measurement is stable (slight probe movements do not significantly alter the guided modes); and (iii) the guided modes measured in both directions are consistent. Next, to further ensure the measurement quality and compensate for this visual inspection, strict post-processing criteria were adopted to classify the measurement as a success or a failure.[40] In short, a series of ten acquisitions is considered as stable and is therefore retained if at least 7 acquisitions are succesful, *i.e.*, provide the two parameters $\mathrm{Ct.Th_{US}}$ and $\mathrm{Ct.Po_{US}}$, and if the corresponding standard deviations are less than two heuristic thresholds fixed to 0.5 mm for $\mathrm{Ct.Th_{US}}$ and 5% for $\mathrm{Ct.Po_{US}}$. Each series corresponds to an intermediate repositioning of the probe. The measurement is considered as valid when at least three series are consistent, *i.e.*, when the differences of the values of each series are less than the two above mentioned thresholds. The final values of the identified waveguide parameters are set to the mean of the values of each successful series. The BDAT measurement on a patient typically lasts 5 to 10 minutes, a time lapse during which the patient is seated with the forearm in a still position on a table.

*Reproducibility*

The inter-operator reproducibility was evaluated by measuring 27 healthy subjects (21 to 55 years old, 16 males and 11 females) by two operators. A written informed consent was provided by the subjects, who were not part of the cohort of patients. Measurements were performed in a blinded fashion, *i.e.*, only one operator was present at the time. Three values were estimated to assess the reproducibility: the root mean square (RMS) average of

the variance of duplicate measurements on the subjects, the intra-class correlation coefficient (ICC), and the standardized coefficient of variation (SCV), which is defined as the ratio of the RMS error by the range of measures given by four times the population standard deviation.[47]

*DXA reference measurements*

DXA measurements of the L2–L4 lumbar spine (aBMD spine), femoral neck (aBMD neck) and total femur (aBMD femur) were performed on patients using two systems of the same manufacturer: Delphi W and QDR 4500A (Hologic Bedford, MA, USA). The two devices have been previously cross-calibrated. The patients were measured the same day by the two techniques, DXA and BDAT.

*Statistical analysis*

Statistical analyses have been performed using the open source programming language R and the Statistics and Machine Learning Toolbox provided by Matlab (MathWorks, Natick, MA USA). Continuous variables were presented as mean with standard deviation. Non-parametric tests were used. For each variable, a Wilcoxon-Mann-Whitney test was performed to determine whether the values were significantly different between the non-fractured group and any fractured group. Note that the statistical tests for QUS and DXA variables were achieved on variables adjusted for age, BMI and glucorticoid treatment. Spearman's rank correlation analysis was used to compare estimates of $\mathrm{Ct.Th_{US}}$ and $\mathrm{Ct.Po_{US}}$ with age, body mass index (BMI) and aBMD values. The level of statistical significance in both tests was determined at a $p$-value below 0.05.

To explore the association between the measured QUS and DXA variables and fragility fracture as a dependent variable, the odds ratios (ORs) were calculated using a binomial logistic regression analysis. ORs are expressed as increases in the estimated fracture risk per one standard deviation decrease for Ct.Th and aBMD or one standard deviation increase for Ct.Po. Receiver operator characteristic (ROC) curves were calculated and the area under the curve (AUC) was determined to examine for differences in the ability of DXA and QUS variables to separate between fracture participants and controls. Adjusted ORs and AUCs

were computed with age, BMI, and glucocorticoid treatment as covariates. Various combinations of QUS parameters and aBMD values were also tested in multiple regression models to determine whether a combination of measured variables was able to improve fracture discrimination over a single variable. ROC analysis of the combined model was performed.

## 3. Results

*Inter-operator reproducibility*

The inter-operator results are shown in Fig. 2. Cortical thickness ranged from 2.8 to 3.9 mm while cortical porosity ranged from 3 to 12%. The RMS average of the variance of duplicate measurements were equal to 0.08 mm and 1.5% for cortical thickness and porosity, respectively. The ICC coefficients were equal to 0.90 and 0.59 for cortical thickness and porosity, respectively. The SCV lead to 4% and 10% for cortical thickness and porosity, respectively.

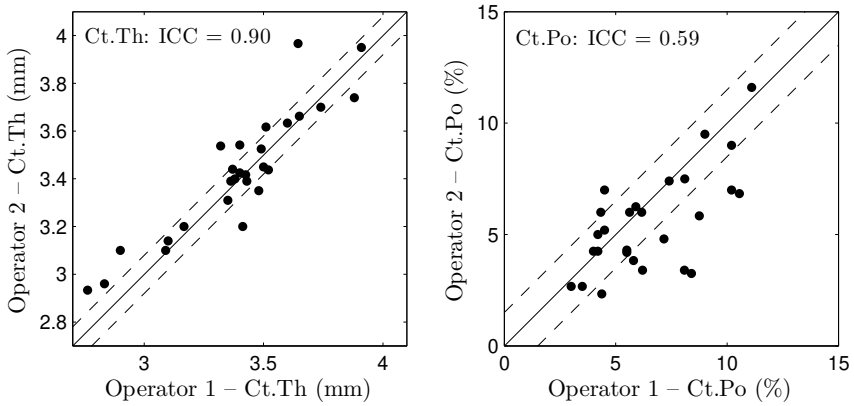


Figure 2: Ct.Th (left) and Ct.Po (right) obtained by the two operators on the 27 healthy subjects of the reproducibility study. Dashed lines correspond to the RMS average of the variance of duplicate measurements, and the ICC is indicated in the upper left corner.

*Measurement failure*

The ultrasonic measurement failed for 49 patients out of 250 (20% of the total cohort). Figure 3 depicts typical measurements for two patients, corresponding to a failure (BMI = 33 kg.m$^{-2}$, non-fractured) and a success (BMI = 18 kg.m$^{-2}$, fractured). Three panels are displayed for each measurement: (i) the time-domain signals (for one emission); (ii) the guided modes (*i.e.*, maxima of the *Norm* function); and (iii) the projected function (Eq.

(2)). As can be observed, a failed measurement is generally associated with the following characteristics: (i) No proper wavefront can be recognized in the time-domain signals, whose waveform results in unexpected wave packets with high amplitude at relatively late arrivals (maybe due to scattering or waves guided in the soft tissue); (ii) poor guided modes; and (iii) a diverging objective function, for which there are no maxima within the explored domain of cortical thickness and porosity values.

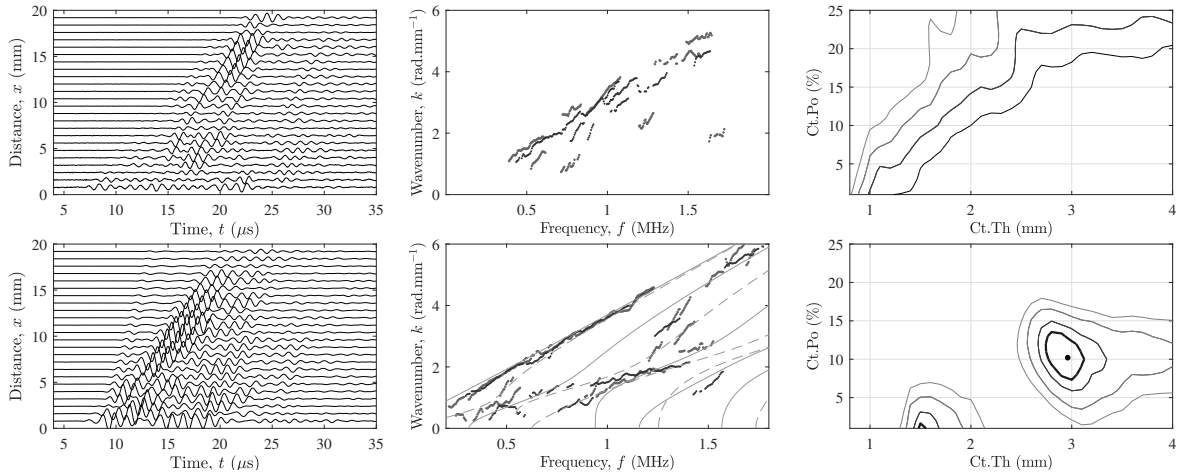


Figure 3: Typical measurements for two patients, corresponding to a failure (upper panels) and a success (lower panels). Three panels are displayed for each measurement: (left) the time-domain signals (for one emission); (middle) the guided modes (*i.e.*, maxima of the *Norm* function); and (right) the projected function (Eq. (2)).

Figure 4 displays the failure rate as a function of BMI together with the BMI distribution. As depicted in Fig. 4(a), the failure rate increased with the BMI. For BMI larger than 28 kg.m$^{-2}$, the failure rate ranged between 55% and 75%. We did not observe any association between measurement failure and presence of fractures.

*Patients' characteristics*

Among the 201 patients for whom the measurements were successful, 109 belong to the control group without fracture (NF), 92 to the group with non-traumatic fractures (F), 17 to the HF group, 32 to the VF group, and 17 to the WF group. Other fracture sites were: humerus, tibia, ankle and rib. The patients' descriptive characteristics are shown in Table 1. Mean age in all fractured groups was higher than in the non-fractured group and with the exception of the HF group the differences were all statistically significant. Note that the

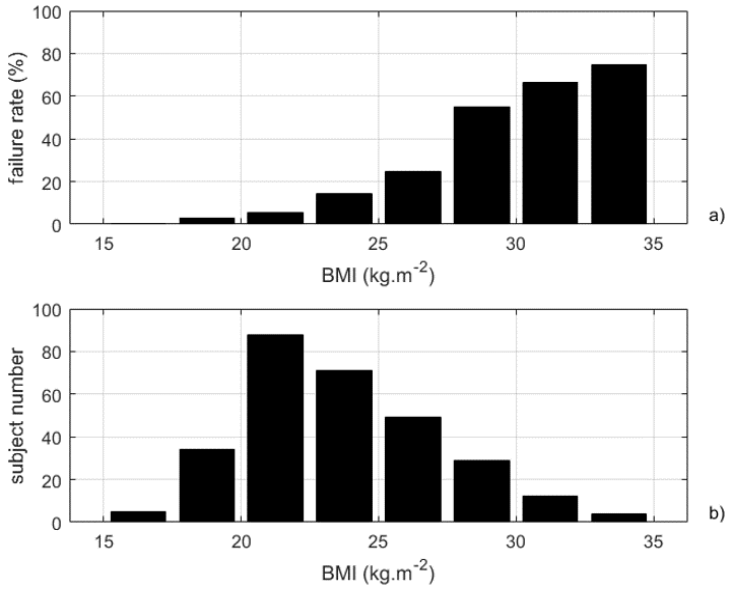


Figure 4: (a) Failure rate (%) vs BMI (kg.m$^{-2}$) and (b) BMI distribution.

relatively young age of the hip fracture group is likely due to the fact that only ambulatory patients were measured with ultrasound.

Table 1: *Descriptive characteristics as mean and standard deviation (*$p < 0.05$ *vs non-fractured group,* **$p < 0.01$ *vs non-fractured group,* ***$p < 0.001$ *vs non-fractured group). Note that the statistical tests for QUS and DXA variables were achieved on variables adjusted for age, BMI and glucorticoid treatment.*

| | **NF (N=109)** | **F (N=92)** | **HF (N=17)** | **VF (N=32)** | **WF (N=17)** |
|---|---|---|---|---|---|
| **Age (years)** | 62.6 (7.8) | 68.8 (9.2)*** | 66.1 (10.3) | 72.4 (7.9)*** | 67.8 (9.6)* |
| **Height (cm)** | 160.0 (6.1) | 158.2 (6.5)* | 160.0 (6.7) | 156.8 (6.4)* | 158.8 (8.3) |
| **Weight (kg)** | 58.8 (8.5) | 57.1 (8.8) | 59.8 (8.8) | 57.9 (9.3) | 56.7 (6.4) |
| **BMI (kg.m$^{-2}$)** | 22.9 (3.1) | 22.8 (3.1) | 23.4 (3.1) | 23.5 (3.5) | 22.5 (1.6) |
| **Ct.Th$_{US}$ (mm)** | 3.02 (0.44) | 2.83 (0.46)* | 2.61 (0.54)*** | 2.87 (0.41)* | 2.91 (0.37) |
| **Ct.Po$_{US}$ (%)** | 10.2 (3.0) | 11.6 (3.5)*** | 9.4 (2.8) | 12.8 (3.3)*** | 12.4 (2.8)*** |
| **aBMD neck (g.cm$^{-2}$)** | 0.661 (0.087) | 0.612 (0.068)*** | 0.607 (0.075)*** | 0.611 (0.069)* | 0.629 (0.053) |
| **aBMD femur (g.cm$^{-2}$)** | 0.783 (0.098) | 0.737 (0.084)* | 0.707 (0.095)*** | 0.747 (0.083) | 0.764 (0.064) |
| **aBMD spine (g.cm$^{-2}$)** | 0.848 (0.181) | 0.833 (0.144) | 0.869 (0.097) | 0.804 (0.142) | 0.878 (0.172) |

aBMD neck was lower in fractured groups (all $p < 0.05$), except in the WF group ($p > 0.05$). The F and HF groups were associated with lower aBMD femur ($p < 0.05$). aBMD spine was not different between fractured and non-fractured groups. Ct.Th$_{US}$ was consistently lower in fractured groups (2.61–2.87 mm; all $p < 0.05$), except in the WF group (2.91 mm; $p > 0.05$) in comparison with the non-fractured group (3.02 mm). Ct.Po$_{US}$ was higher in all fractured groups (11.6–12.8%; all $p < 0.001$), except in the HF group (9.4%; $p > 0.05$)

compared to the non-fractured group (10.2%). Note that a lower height was observed in the F and VF groups ($p < 0.05$) while no difference existed in BMI and weight between groups.

*Spearman's rank correlation analysis*

The correlation results are summarized in Table 2. aBMD femur, aBMD neck and aBMD spine were all correlated (R from 0.46 to 0.84; all $p < 0.001$). There was no correlation between $Ct.Th_{US}$ and $Ct.Po_{US}$. Weak correlations were observed between QUS and DXA results (R around 0.20; $p < 0.01$). $Ct.Th_{US}$ was not correlated with aBMD spine, whereas a weak correlation was observed for $Ct.Po_{US}$ ($R = 0.16$; $p < 0.05$). All QUS and DXA variables were correlated with age and BMI. The correlation of $Ct.Th_{US}$ to age is negative, while it is positive for $Ct.Po_{US}$. Age and BMI were not correlated.

Table 2: *Spearman's correlation coefficients R between US variables, aBMD, age and BMI (*$p < 0.05$, **$p < 0.01$, ***$p < 0.001$).*

| | **$Ct.Th_{US}$** | **$Ct.Po_{US}$** | **aBMD neck** | **aBMD femur** | **aBMD spine** | **Age** | **BMI** |
|---|---|---|---|---|---|---|---|
| **$Ct.Th_{US}$** | – | -0.01 | 0.23** | 0.19** | 0.07 | -0.35*** | 0.29*** |
| **$Ct.Po_{US}$** | -0.01 | – | -0.15* | -0.12 | -0.16* | 0.16* | -0.27*** |
| **aBMD neck** | 0.23** | -0.15* | – | 0.84*** | 0.46*** | -0.44*** | 0.33*** |
| **aBMD femur** | 0.19** | -0.12 | 0.84*** | – | 0.56*** | -0.40*** | 0.36*** |
| **aBMD spine** | 0.07 | -0.16* | 0.46*** | 0.56*** | – | -0.21** | 0.30*** |
| **Age** | -0.35*** | 0.16* | -0.44*** | -0.40*** | -0.21** | – | 0.00 |
| **BMI** | 0.29*** | -0.27*** | 0.33*** | 0.36*** | 0.30*** | 0.00 | – |

*Fracture discrimination*

Systematic adjustment for age, BMI and glucocorticoid treatment was made for all the analyses. The results of the logistic regression analysis and AUCs are shown in Table 3. Results for the adjusted variables are as follows. aBMD neck was discriminant for all non-traumatic fractures combined (AUC: 0.72; OR: 1.48) and marginally discriminant for hip fractures ($p = 0.063$). aBMD femur was discriminant for hip fracture only (AUC = 0.70; OR = 2.21). Lumbar spine aBMD was not discriminant for any fractured group. VF and WF groups could not be discriminated with any aBMD variable.

With the exception of the HF group, $Ct.Po_{US}$ could discriminate all fractured groups from the non-fractured group (AUCs: 0.71–0.84; ORs: 1.39–1.96), whereas $Ct.Th_{US}$ was discriminant for hip fractures only (AUC: 0.72; OR: 2.01). For all non-traumatic fractures combined and hip fractures, aBMD neck performed slightly better than QUS parameters in

terms of AUCs and ORs. For vertebral and wrist fractures, $Ct.Po_{US}$ was the only significant discriminator, with AUCs equal to 0.84 (VF) and 0.71 (WF) and ORs equal to 1.96 (VF) and 1.80 (WF), respectively. The magnitude of changes reached with a combination of QUS variables or a combination of QUS and aBMD variables was limited. $Ct.Po_{US}$ was found to be associated with all non-traumatic fractures combined independently from aBMD neck, while $Ct.Th_{US}$ was found to be associated with hip fracture independently from aBMD femur. Apart from the combination of aBMD femur and $Ct.Th_{US}$ weakly improving AUC from 0.72 to 0.74 (albeit nonsignificant) in case of hip fractures, there was no improvement in fracture risk prediction when combining different variables.

## 4. Discussion

This pilot study investigated the ability of two QUS cortical parameters, Ct.Th and Ct.Po, estimated from measurements at the one-third distal radius using a custom-made guided wave technology to discriminate postmenopausal women with non-traumatic fractures from the control group. The main findings from this study were that (i) Ct.Po was discriminant for all non-traumatic fractures combined and, in particular, for vertebral and wrist fractures, while Ct.Th was discriminant for hip fractures only; (ii) the demonstration of a significant association between increased porosity at the one-third distal radius assessed by BDAT and vertebral and wrist fractures when these fractures were not associated with any measured aBMD variables; (iii) the association between increased cortical porosity and all non-traumatic fractures combined independently of aBMD neck; and (iv) the association between decreased cortical thickness and hip fractures independently of aBMD femur.

To the best of our knowledge, this study reports for the first time on the concurrent *in vivo* estimates of two cortical bone quality markers, *i.e.*, cortical thickness and porosity, using an ultrasound modality based on the propagation of guided waves, and their association with fractures. Some earlier studies have reported on fracture discrimination with ultrasound AT measurements at high ($\sim$ 1.0 MHz) or low frequencies ($\sim$ 250 kHz) on the radius or tibia.[21,22,24,48–50] Unlike these earlier studies relying on the FAS velocity, the estimated QUS parameters were here not directly measured but derived from a model-based inverse problem approach that was previously validated. This procedure, applied *in vivo* at the one-third distal radius of healthy subjects, yielded thickness estimates in good agreement with

ground truth values derived from site-matched HR-pQCT measurements.[41] In addition, both Ct.Th and Ct.Po have been recently validated against traditional $\mu$-CT on *ex vivo* bone specimens.[40] Our Ct.Th values ranging from 1.6 to 3.9 mm are consistent with values obtained *in vivo* at the same site, *i.e.*, the one-third distal radius, using pulse-echo[51,52] or pQCT.[49] However, as no *in vivo* porosity measurement using QUS have been reported so far, our Ct.Po values, ranging from 3 to 21%, can only be compared with *ex vivo* reference values, obtained at the same site using synchrotron $\mu$-CT[53] or scanning acoustic microscopy.[54] It is also worth mentioning that ultrasound waves are elastic waves, which are sensitive to the effective elastic properties of the propagation medium. The effective elastic properties, *i.e.*, the homogenized elastic properties at the mm length scale, are partly determined by the microstructure. Therefore, in principle, our Ct.Po estimates reflect the porosity below the resolution limit of HR-pQCT.

QUS parameters could not be identified for 49 patients, and the failure rate (around 20%) was typically associated with higher BMI, as it was already evidenced in earlier studies relying on the FAS velocity.[23,48] Higher BMI implies a thicker soft tissue layer on top of bone, which complicates probe alignment with the main bone axis, entails higher signal attenuation and generates the presence of unwanted additional guided modes propagating in the soft tissue layer. Identification of cortical bone properties in presence of thick soft tissue may be challenging and may require more sophisticated models than the one used here.[55] The general complexity of cortical bone structure, and particularly the disruption of the endosteal bone edge and the presence of large resorption cavities that can be observed in case of strongly deteriorated bones,[56] may impact the generation and propagation of guided waves.[40] However, in this study the failure rate was not correlated with fracture history.

With the renewed interest in assessing *in vivo* the cortical compartment,[56] which has long been neglected, new techniques that measure critical indices beyond aBMD directly related to fracture risk such as cortical porosity and thickness have flourished in recent years. So far, the current gold standard for cortical micro-architecture assessment at the radius is HR-pQCT, which also provides estimates of Ct.Th and Ct.Po.[10] However, HR-pQCT is limited to clinical research facilities and will unlikely be used as a widespread diagnostic tool for osteoporosis due to cost issues and ionizing radiations. With the advantage of non-

invasiveness and affordability, compact ultrasound devices that measure forearm (radius) or leg (tibia) cortical bone is a vivid research area.[16,41,49,51,57]

Central DXA measurements, performed at the lumbar spine, femoral neck and total femur, delivered reference aBMD values that serve as the gold standard for skeletal status assessment. At the vertebral site, aBMD values could not discriminate between controls and fractured subjects. This may be due to the small number ($n = 32$) of vertebral fractures. At the femoral site, aBMD neck and aBMD femur differed between controls and all non-traumatic fractures combined, however aBMD neck was the only parameter able to discriminate hip fractures from controls, which may be an effect of the small sample size. Similar results have been reported in other cohort population studies.[58]

First, our results showed that Ct.Th and Ct.Po, as depicted by BDAT, exhibited significant age-related dependence for females: concurrent to the increased porosity, the thickness at the radius was reduced with aging. These results are consistent with data obtained previously with HR-pQCT.[10,56,59–63] Second, Ct.Th and Ct.Po were associated with fracture. There are no equivalent studies comparable to ours; however, many cross-sectional and retrospective studies have evaluated the association of HR-pQCT-derived cortical structural variables, Ct.Th and Ct.Po, measured at the ultradistal radius, with odds of prior fracture in women. These studies have demonstrated that alterations of cortical bone structure at the ultradistal radius, such as low Ct.Th[58,64–71] or high Ct.Po,[72,73] are associated with prevalent fracture. In a few studies, the association between Ct.Th and the existence of fractures remained significant even after adjustment for aBMD.[64,69]

All these previous studies rely on HR-pQCT, but only a few reports rely on the measurement of cortical thickness with QUS modalities. Mishima *et al.*[57] reported that Ct.Th measured in ultrasound transmission at the ultradistal radius was a significant factor independently associated with vertebral fractures in type 2 diabetes mellitus patients with low estimated glomerular filtration rate. The ability of Ct.Th measured at the radius or tibia with pulse-echo ultrasonometry and combined with patient characteristics (age, weight, and height) to discriminate postmenopausal patients with osteoporosis from those without osteoporosis (as measured by DXA of the hip) was reported by Schousboe *et al.*[52] In the same study, a significant association of tibial (but not radial) Ct.Th with all types of prior fractures

was found.

In our study, guided waves measurements presented adjusted ORs and AUCs of comparable magnitude to aBMD measurements for all non-traumatic fractures combined and hip fractures. Interestingly, Ct.Th and Ct.Po were associated with fractures of different groups (Ct.Th for the HF group and Ct.Po for the VF and WF groups), suggesting the capability of QUS-based estimates of cortical bone structure characteristics to predict site-specific fracture risk. Furthermore, Ct.Po could discriminate the vertebral and wrist fractured groups from controls, when these two groups could not be discriminated using aBMD and an association between Ct.Po and all non-traumatic fractures combined, as well as between Ct.Th and hip fractures, independent of aBMD was observed. However, whether a combination of variables, ultrasonic or densitometric, could yield a better discrimination in comparison to a variable alone could not be demonstrated here. Our results confirm previous studies that showed alterations of cortical bone structure in subjects with fracture, and that these alterations are associated with hip, vertebral, wrist or all type of fragility fractures. However, altogether, the results of these studies and those of our study do not all concur on the discriminating ability of cortical thickness or porosity measured at the radius for different fracture skeletal sites and on the aBMD-independent association of these parameters after adjustment on the aBMD. Likely source of these discrepancies is the limited number of fractures in most studies. Furthermore, the region investigated with HR-pQCT is more distal than the one investigated with QUS, which calls for caution for the comparison of HR-pQCT and AT studies. To the best of our knowledge, there is only one report showing the ability of cortical thickness measured at the one-third distal radius (using pQCT) to retrospectively discriminate postmenopausal subjects with all types of low- or moderate-energy fracture from non-fractured subjects, with OR=1.51 and AUC=0.78 similar to ours.[49]

Our study had several limitations. A first limitation is the overall small number of patients and particularly the small number of fractures in each group. This pilot study with 20 to 30 fractured women in each fracture group may have been underpowered to provide robust estimates. Larger studies are needed to address the question of whether cortical thickness and porosity can be used as site-specific fracture risk factors and whether these parameters are risk indicators of fracture independent of aBMD, particularly in patients with normal

aBMD, or if it offers additional discriminatory capacity over aBMD in a particular category of patients. In that vein, it would also be valuable to account for the number of vertebral fractures and fracture severity in the analysis. Nonetheless, such approach was not conducted here, because of the low sample sizes of the different sub-groups. A second limitation is that in absence of DXA measurements at the distal radius, we could not test whether, after adjusting for radial aBMD, differences between women with fracture and controls remained significant for the QUS variables, in particular for wrist fractures. Third, for sake of comparison with previous scans, our center continues analyzing only L2 to L4 vertebrae. However, to be consistent with most studies, analyzing L1 to L4 vertrebrae could lead to improved fracture discrimination of the VF group. This has to be taken into account in further studies. Fourth, BDAT measurements were done retrospectively after the fractures were sustained. The independent contribution of cortical structure as depicted by ultrasound to the risk of fracture has to be evaluated prospectively. Fifth, the free plate model used for cortical bone characteristics identification was parametrized in terms of thickness and porosity, assuming universal material properties of the tissue matrix. Fixed matrix properties did not take into account the inevitable inter-individual variability of bone tissue properties.[74] However, such a hypothesis has been found to yield reasonably accurate *ex vivo* identification of Ct.Th and Ct.Po of human radius and tibia specimens.[40] This model simplification can be avoided using a model parametrized in terms of thickness and stiffness (*i.e.*, including four independent stiffness coefficients to account for the generally accepted transverse isotropy of cortical long bones measured axially). Our group achieved concurrent estimates of both thickness and bulk wave velocities (directly reflecting the elastic properties) of cortical bone using such a transverse isotropic plate model.[37,55] However, as experimental dispersion curves are usually incomplete and noisy, solving such a multiparametric inverse problem could lead to an ill-posed inversion (*i.e.*, numerous local optima) and overfitting of the data. To make this technique available in clinical studies, simplifications of the model are currently required to reduce computing time and ensure robustness of parameters identification. An important current limitation of our BDAT approach is that it fails when the thickness of soft tissue is large (*i.e.*, typically associated with BMI larger than 28 $kg.m^{-2}$ in this study). Further research is warranted to make this technology available to patients with BMI above 28 $kg.m^{-2}$. The

focus will be on the improvement of the HMI (by including quantitative features delivering a real time feedback on the probe alignment) and on the development of more sophisticated waveguide models accounting for the soft tissue layer (whose thickness could be evaluated by conventional pulse-echo imaging for instance). Finally, the prototype status of the device should be considered when interpreting the results. The role of the operator in data acquisition is critical. At this stage, the operator ability to correctly align the probe along the main bone axis is a key issue for the measurement success. The measurement protocol has been carefully designed to guide the operator and optimize the measurement reproducibility, but it is expected that ongoing developments of the probe, the HMI and the methodology may lead to improved fracture discrimination in the future. Reproducibility studies on patients are currently being conducted in different healthcare centers with an updated version of the HMI.

## 5. Conclusion

In summary, our results indicate that BDAT measurements at the one-third distal radius may be used to characterize cortical bone in postmenopausal women. Ct.Po was discriminant for all non-traumatic fractures combined and, in particular, vertebral and wrist fractures when these fractures were not associated with any measured aBMD variables, while Ct.Th was discriminant for hip fractures only. These results open perspectives to the clinical assessment of cortical bone using a portable and non-ionizing device.

## Acknowledgment

This work received financial support from the Fondation pour la Recherche Médicale (FRM DBS201311228444), MSD and Azalée.

Authors' roles: Study design: PL and CR. Patient recruitment: SK, KB, and CR. US reproducibility study: DR and JGM. US data collection: QV, NB, and JGM. Data analysis: DR and JGM. Drafting manuscript: JGM and DR. Revising manuscript content: All authors. AE and JGM take responsibility for the integrity of the data analysis.

## References

1. Seeman E, Delmas P. Bone quality–the material and structural basis of bone strength and fragility. N Engl J Med. 2006;354(21):2250–2261.

2. Curtis E, Moon R, Harvey N, Cooper C. The impact of fragility fracture and approaches to osteoporosis risk assessment worldwide. Bone. 2017;104:29–38.

3. Haentjens P, Magaziner J, Colón-Emeric C, Vanderschueren D, Milisen K, Velkeniers B, et al. Meta-analysis: excess mortality after hip fracture among older women and men. Ann Intern Med. 2010;152(6):380–390.

4. Van Den Bergh J, Van Geel T, Geusens P. Osteoporosis, frailty and fracture: implications for case finding and therapy. Nat Rev Rheumatol. 2012;8(3):163.

5. Kanis J, Johnell O, Oden A, Dawson A, De Laet C, Jonsson B. Ten year probabilities of osteoporotic fractures according to BMD and diagnostic thresholds. Osteoporos Int. 2001;12(12):989–995.

6. Siris E, Chen YT, Abbott T, Barrett-Connor E, Miller P, Wehren L, et al. Bone mineral density thresholds for pharmacological intervention to prevent fractures. Arch Intern Med. 2004;164(10):1108–1112.

7. Geusens P, Van Geel T, Huntjens K, Van Helden S, Bours S, Van Den Bergh J. Clinical fractures beyond low BMD. Int J Clin Rheumtol. 2011;6(4):411.

8. Lespessailles E, Cortet B, Legrand E, Guggenbuhl P, Roux C. Low-trauma fractures without osteoporosis. Osteoporos Int. 2017;28(6):1771–1778.

9. Shigdel R, Osima M, Ahmed L, Joakimsen R, Eriksen E, Zebaze R, et al. Bone turnover markers are associated with higher cortical porosity, thinner cortices, and larger size of the proximal femur and non-vertebral fractures. Bone. 2015;81:1–6.

10. Nishiyama K, Macdonald H, Buie H, Hanley D, Boyd S. Postmenopausal women with osteopenia have higher cortical porosity and thinner cortices at the distal radius and tibia than women with normal aBMD: an in vivo HR-pQCT study. J Bone Miner Res. 2010;25(4):882–890.

11. Augat P, Schorlemmer S. The role of cortical bone and its microstructure in bone strength. Age Ageing. 2006;35(suppl_2):ii27–ii31.

12. Bala Y, Zebaze R, Seeman E. Role of cortical bone in bone fragility. Curr Opin Rheumatol. 2015;27(4):406–413.

13. Cooper D, Kawalilak C, Harrison K, Johnston B, Johnston J. Cortical Bone Porosity: What Is It, Why Is It Important, and How Can We Detect It? Curr Osteoporos Rep. 2016;14(5):187–198.

14. Zebaze R, Ghasem-Zadeh A, Mbala A, Seeman E. A new method of segmentation of compact-appearing, transitional and trabecular compartments and quantification of cortical porosity from high resolution peripheral quantitative computed tomographic images. Bone. 2013;54(1):8–20.

15. Diez-Perez A, Güerri R, Nogues X, Cáceres E, Peña M, Mellibovsky L, et al. Microindentation for in vivo measurement of bone tissue mechanical properties in humans. J Bone Miner Res. 2010;25(8):1877–1885.

16. Stein E, Rosete F, Young P, Kamanda-Kosseh M, McMahon D, Luo G, et al. Clinical assessment of the 1/3 radius using a new desktop ultrasonic bone densitometer. Ultrasound Med Biol. 2013;39(3):388–395.

17. Sai H, Iguchi G, Tobimatsu T, Takahashi K, Otani T, Horii K, et al. Novel ultrasonic bone densitometry based on two longitudinal waves: significant correlation with pQCT measurement values and age-related changes in trabecular bone density, cortical thickness, and elastic modulus of trabecular bone in a normal Japanese population. Osteoporos Int. 2010;21(10):1781–1790.

18. Mano I, Horii K, Hagino H, Miki T, Matsukawa M, Otani T. Estimation of in vivo cortical bone thickness using ultrasonic waves. J Med Ultrason. 2015;42(3):315–322.

19. Talmant M, Foiret J, Minonzio JG. Guided waves in cortical bone. In: Bone quantitative ultrasound. Springer; 2011. p. 147–179.

20. Hans D, Baim S. Quantitative Ultrasound (QUS) in the management of osteoporosis and assessment of fracture risk. J Clin Densitom. 2017;20(3):322–333.

21. Foldes A, Rimon A, Keinan D, Popovtzer M. Quantitative ultrasound of the tibia: a novel approach for assessment of bone status. Bone. 1995;17(4):363–367.

22. Barkmann R, Kantorovich E, Singal C, Hans D, Genant H, Heller M, et al. A new method for quantitative ultrasound measurements at multiple skeletal sites: first results of precision and fracture discrimination. J Clin Densitom. 2000;3(1):1–7.

23. Weiss M, Ben-Shlomo A, Hagag P, Rapoport M. Reference database for bone speed of sound measurement by a novel quantitative multi-site ultrasound device. Osteoporos Int. 2000;11(8):688–696.

24. Knapp K, Blake G, Spector T, Fogelman I. Multisite quantitative ultrasound: precision, age-and menopause-related changes, fracture discrimination, and T-score equivalence with dual-energy X-ray absorptiometry. Osteoporos Int. 2001;12(6):456–464.

25. Olszynski W, Brown J, Adachi J, Hanley D, Ioannidis G, Davison K, et al. Multisite quantitative ultrasound for the prediction of fractures over 5 years of follow-up: The Canadian Multicentre Osteoporosis Study. J Bone Miner Res. 2013;28(9):2027–2034.

26. Nicholson P, Moilanen P, Kärkkäinen T, Timonen J, Cheng S. Guided ultrasonic waves in long bones: modelling, experiment and in vivo application. Physiol Meas. 2002;23(4):755.

27. Moilanen P. Ultrasonic guided waves in bone. IEEE Trans Ultrason Ferroelectr Freq Control. 2008;55(6).

28. Moilanen P, Nicholson P, Kilappa V, Cheng S, Timonen J. Assessment of the cortical bone thickness using ultrasonic guided waves: Modelling and in vitro study. Ultrasound Med Biol. 2007;33(2):254–262.

29. Minonzio JG, Talmant M, Laugier P. Guided wave phase velocity measurement using multi-emitter and multi-receiver arrays in the axial transmission configuration. J Acoust Soc Am. 2010;127(5):2913–2919.

30. Tran T, Nguyen KC, Sacchi M, Le L. Imaging ultrasonic dispersive guided wave energy in long bones using linear radon transform. Ultrasound Med Biol. 2014;40(11):2715–2727.

31. Xu K, Ta D, Cassereau D, Hu B, Wang W, Laugier P, et al. Multichannel processing for dispersion curves extraction of ultrasonic axial-transmission signals: Comparisons and case studies. J Acoust Soc Am. 2016;140(3):1758–1770.

32. Okumura S, Nguyen VH, Taki H, Haïat G, Naili S, Sato T. Rapid High-Resolution Wavenumber Extraction from Ultrasonic Guided Waves Using Adaptive Array Signal Processing. Appl Sci. 2018;8(4).

33. Moilanen P, Talmant M, Kilappa V, Nicholson P, Cheng S, Timonen J, et al. Modeling the impact of soft tissue on axial transmission measurements of ultrasonic guided waves in human radius. J Acoust Soc Am. 2008;124(4):2364–2373.

34. Ta D, Wang W, Wang Y, Le L, Zhou Y. Measurement of the dispersion and attenuation of cylindrical ultrasonic guided waves in long bone. Ultrasound Med Biol. 2009;35(4):641–652.

35. Nguyen VH, Tran T, Sacchi M, Naili S, Le L. Computing dispersion curves of elastic/viscoelastic transversely-isotropic bone plates coupled with soft tissue and marrow using semi-analytical finite element (SAFE) method. Comput Biol Med. 2017;87:371–381.

36. Lefebvre F, Deblock Y, Campistron P, Ahite D, Fabre J. Development of a new ultrasonic technique for bone and biomaterials in vitro characterization. J Biomed Mater Res A. 2002;63(4):441–446.

37. Foiret J, Minonzio JG, Chappard C, Talmant M, Laugier P. Combined estimation of thickness and velocities using ultrasound guided waves: A pioneering study on in vitro cortical bone samples. IEEE Trans Ultrason Ferroelect Freq Control. 2014;61(9):1478–1488.

38. Bochud N, Vallet Q, Bala Y, Follet H, Minonzio J, Laugier P. Genetic algorithms-based inversion of multimode guided waves for cortical bone characterization. Phys Med Biol. 2016;61(19):6953.

39. Bossy E, Talmant M, Defontaine M, Patat F, Laugier P. Bidirectional axial transmission can improve accuracy and precision of ultrasonic velocity measurement in cortical

bone: A validation on test materials. IEEE Trans Ultrason Ferroelect Freq Control. 2004;51(1):71–79.

40. Minonzio JG, Bochud N, Vallet Q, Bala Y, Ramiandrisoa D, Follet H, et al. Bone cortical thickness and porosity assessment using ultrasound guided waves: An ex vivo validation study. Bone. 2018;116:111–119.

41. Vallet Q, Bochud N, Chappard C, Laugier P, Minonzio JG. In vivo characterization of cortical bone using guided waves measured by axial transmission. IEEE Trans Ultrason Ferroelect Freq Control. 2016;63(9):1361–1371.

42. Warriner A, Patkar N, Curtis J, Delzell E, Gary L, Kilgore M, et al. Which fractures are most attributable to osteoporosis? J Clin Epidemiol. 2011;64(1):46–53.

43. Moreau L, Minonzio JG, Foiret J, Bossy E, Talmant M, Laugier P. Accurate measurement of guided modes in a plate using a bidirectional approach. J Acoust Soc Am. 2014;135(1):EL15–EL21.

44. Minonzio JG, Foiret J, Talmant M, Laugier P. Impact of attenuation on guided mode wavenumber measurement in axial transmission on bone mimicking plates. J Acoust Soc Am. 2011;130(6):3574–3582.

45. Granke M, Grimal Q, Saïed A, Nauleau P, Peyrin F, Laugier P. Change in porosity is the major determinant of the variation of cortical bone elasticity at the millimeter scale in aged women. Bone. 2011;49(5):1020–1026.

46. Parnell W, Vu M, Grimal Q, Naili S. Analytical methods to determine the effective mesoscopic and macroscopic elastic properties of cortical bone. Biomech Model Mechanobiol. 2012;11(6):883–901.

47. Orgee J, Foster H, McCloskey E, Khan S, Coombes G, Kanis J. A precise method for the assessment of tibial ultrasound velocity. Osteoporos Int. 1996;6(1):1–7.

48. Talmant M, Kolta S, Roux C, Haguenauer D, Vedel I, Cassou B, et al. In vivo performance evaluation of bi-directional ultrasonic axial transmission for cortical bone assessment. Ultrasound Med Biol. 2009;35(6):912–919.

49. Moilanen P, Määttä M, Kilappa V, Xu L, Nicholson P, Alén M, et al. Discrimination of fractures by low-frequency axial transmission ultrasound in postmenopausal females. Osteoporos Int. 2013;24(2):723–730.

50. Määttä M, Moilanen P, Timonen J, Pulkkinen P, Korpelainen R, Jämsä T. Association between low-frequency ultrasound and hip fractures-comparison with DXA-based BMD. BMC Musculoskelet Disord. 2014;15(1):208.

51. Karjalainen J, Riekkinen O, Töyräs J, Jurvelin J, Kröger H. New method for point-of-care osteoporosis screening and diagnostics. Osteoporos Int. 2016;27(3):971–977.

52. Schousboe J, Riekkinen O, Karjalainen J. Prediction of hip osteoporosis by DXA using a novel pulse-echo ultrasound device. Osteoporos Int. 2017;28(1):85–93.

53. Bossy E, Talmant M, Peyrin F, Akrout L, Cloetens P, Laugier P. An in vitro study of the ultrasonic axial transmission technique at the radius: 1-MHz velocity measurements are sensitive to both mineralization and intracortical porosity. J Bone Miner Res. 2004;19(9):1548–1556.

54. Raum K, Leguerney I, Chandelier F, Bossy E, Talmant M, Saïed A, et al. Bone microstructure and elastic tissue properties are reflected in QUS axial transmission measurements. Ultrasound Med Biol. 2005;31(9):1225–1235.

55. Bochud N, Vallet Q, Minonzio JG, Laugier P. Predicting bone strength with ultrasonic guided waves. Sci Rep. 2017;7:43628.

56. Zebaze R, Ghasem-Zadeh A, Bohte A, Iuliano-Burns S, Mirams M, Price R, et al. Intracortical remodelling and porosity in the distal radius and post-mortem femurs of women: a cross-sectional study. The Lancet. 2010;375(9727):1729–1736.

57. Mishima T, Motoyama K, Imanishi Y, Hamamoto K, Nagata Y, Yamada S, et al. Decreased cortical thickness, as estimated by a newly developed ultrasound device, as a risk for vertebral fracture in type 2 diabetes mellitus patients with eGFR of less than 60 mL/min/1.73 m2. Osteoporos Int. 2015;26(1):229–236.

58. Vico L, Zouch M, Amirouche A, Frère D, Laroche N, Koller B, et al. High-resolution pQCT analysis at the distal radius and tibia discriminates patients with recent wrist and femoral neck fractures. J Bone Miner Res. 2008;23(11):1741–1750.

59. Nicks K, Amin S, Atkinson E, Riggs B, Melton L, Khosla S. Relationship of age to bone microstructure independent of areal bone mineral density. J Bone Miner Res. 2012;27(3):637–644.

60. Bala Y, Zebaze R, Ghasem-Zadeh A, Atkinson E, Iuliano S, Peterson J, et al. Cortical porosity identifies women with osteopenia at increased risk for forearm fractures. J Bone Miner Res. 2014;29(6):1356–1362.

61. Shanbhogue V, Brixen K, Hansen S. Age-and sex-related changes in bone microarchitecture and estimated strength: a three-year prospective study using HRpQCT. J Bone Miner Res. 2016;31(8):1541–1549.

62. Vilayphiou N, Boutroy S, Sornay-Rendu E, Van Rietbergen B, Chapurlat R. Age-related changes in bone strength from HR-pQCT derived microarchitectural parameters with an emphasis on the role of cortical porosity. Bone. 2016;83:233–240.

63. Alvarenga J, Fuller H, Pasoto S, Pereira R. Age-related reference curves of volumetric bone density, structure, and biomechanical parameters adjusted for weight and height in a population of healthy women: an HR-pQCT study. Osteoporos Int. 2017;28(4):1335–1346.

64. Boutroy S, Khosla S, Sornay-Rendu E, Zanchetta M, McMahon D, Zhang C, et al. Microarchitecture and peripheral BMD are impaired in postmenopausal white women with fracture independently of total hip T-score: an international multicenter study. J Bone Miner Res. 2016;31(6):1158–1166.

65. Boutroy S, Van Rietbergen B, Sornay-Rendu E, Munoz F, Bouxsein M, Delmas P. Finite element analysis based on in vivo HR-pQCT images of the distal radius is associated with wrist fracture in postmenopausal women. J Bone Miner Res. 2008;23(3):392–399.

66. Nishiyama K, Macdonald H, Hanley D, Boyd S. Women with previous fragility fractures can be classified based on bone microarchitecture and finite element analysis measured with HR-pQCT. Osteoporos Int. 2013;24(5):1733–1740.

67. Melton L, Christen D, Riggs B, Achenbach S, Müller R, van Lenthe G, et al. Assessing forearm fracture risk in postmenopausal women. Osteoporos Int. 2010;21(7):1161–1169.

68. Zhu T, Hung V, Cheung WH, Cheng J, Qin L, Leung KS. Value of Measuring Bone Microarchitecture in Fracture Discrimination in Older Women with Recent Hip Fracture: A Case-control Study with HR-pQCT. Sci Rep. 2016;6:34185.

69. Sornay-Rendu E, Cabrera-Bravo JL, Boutroy S, Munoz F, Delmas P. Severity of vertebral fractures is associated with alterations of cortical architecture in postmenopausal women. J Bone Miner Res. 2009;24(4):737–743.

70. Wang J, Stein E, Zhou B, Nishiyama K, Yu Y, Shane E, et al. Deterioration of trabecular plate-rod and cortical microarchitecture and reduced bone stiffness at distal radius and tibia in postmenopausal women with vertebral fractures. Bone. 2016;88:39–46.

71. Sornay-Rendu E, Boutroy S, Duboeuf F, Chapurlat R. Bone microarchitecture assessed by HR-pQCT as predictor of fracture risk in postmenopausal women: the OFELY study. J Bone Miner Res. 2017;32(6):1243–1251.

72. Bala Y, Bui Q, Wang XF, Iuliano S, Wang Q, Ghasem-Zadeh A, et al. Trabecular and cortical microstructure and fragility of the distal radius in women. J Bone Miner Res. 2015;30(4):621–629.

73. Edwards M, Robinson D, Ward K, Javaid M, Walker-Bone K, Cooper C, et al. Cluster analysis of bone microarchitecture from high resolution peripheral quantitative computed tomography demonstrates two separate phenotypes associated with high fracture risk in men and women. Bone. 2016;88:131–137.

74. Unal M, Creecy A, Nyman J. The Role of Matrix Composition in the Mechanical Behavior of Bone. Curr Osteoporos Rep. 2018;16(3):205–215.

Table 3: *Odds ratios (ORs) and areas under the ROC curve (AUCs) (Reference category is NF (N=109). CI confidence interval. ROC receiver operating characteristic. AUCs and ORs are adjusted for age, BMI and glucorticoid treatment. The p values of significant results are indicated in bold:* $^{*}p < 0.05$, $^{**}p < 0.01$, $^{***}p < 0.001$*).*

| | **All non-traumatic fractures (N=92)** | | | **Hip fractures (N=17)** | | | **Vertebral fractures (N=32)** | | | **Wrist fractures (N=17)** | | |
|---|---|---|---|---|---|---|---|---|---|---|---|---|
| | AUC [95% CI] | OR [95% CI] | *p* | AUC [95% CI] | OR [95% CI] | *p* | AUC [95% CI] | OR [95% CI] | *p* | AUC [95% CI] | OR [95% CI] | *p* |
| US parameters | | | | | | | | | | | | |
| $Ct.Th_{US}$ | 0.63 [0.56-0.71] | 1.46 [1.09-1.94]$^{**}$ | **0.008** | 0.72 [0.59-0.83] | 1.92 [1.22-3.01]$^{**}$ | **0.004** | 0.62 [0.51-0.71] | 1.36 [0.92-2.01] | 0.113 | 0.60 [0.47-0.75] | 1.25 [0.76-2.05] | 0.375 |
| $Ct.Po_{US}$ | 0.62 [0.55-0.69] | 1.47 [1.12-1.95]$^{**}$ | **0.005** | 0.56 [0.39-0.71] | 1.28 [0.74-2.21] | 0.359 | 0.70 [0.59-0.80] | 2.02 [1.34-3.05]$^{***}$ | $\mathbf{< 10^{-3}}$ | 0.69 [0.57-0.82] | 1.97 [1.14-3.42]$^{*}$ | **0.014** |
| aBMD variables | | | | | | | | | | | | |
| aBMD neck | 0.65 [0.56-0.72] | 1.88 [1.32-2.66]$^{***}$ | $\mathbf{< 10^{-3}}$ | 0.69 [0.54-0.79] | 1.92 [1.03-3.58]$^{*}$ | **0.035** | 0.64 [0.53-0.75] | 1.86 [1.15-3.03]$^{*}$ | **0.010** | 0.60 [0.42-0.73] | 1.45 [0.81-2.61] | 0.203 |
| aBMD femur | 0.61 [0.52-0.68] | 1.59 [1.15-2.19]$^{**}$ | **0.004** | 0.68 [0.53-0.79] | 2.07 [1.15-3.73]$^{*}$ | **0.014** | 0.59 [0.48-0.68] | 1.41 [0.91-2.18] | 0.112 | 0.55 [0.40-0.69] | 1.20 [0.69-2.10] | 0.503 |
| aBMD spine | 0.52 [0.44-0.60] | 1.10 [0.80-1.51] | 0.542 | 0.57 [0.44-0.71] | 1.12 [0.66-1.92] | 0.659 | 0.56 [0.42-0.66] | 1.30 [0.84-2.02] | 0.236 | 0.53 [0.37-0.71] | 1.17 [0.70-1.97] | 0.541 |
| Adjusted US parameters | | | | | | | | | | | | |
| $Ct.Th_{US}$ | 0.70 [0.62-0.77] | 1.18 [0.85-1.63] | 0.317 | 0.72 [0.51-0.85] | 2.01 [1.22-3.33]$^{**}$ | **0.005** | 0.82 [0.75-0.89] | 1.07 [0.66-1.75] | 0.777 | 0.67 [0.49-0.80] | 1.02 [0.57-1.82] | 0.939 |
| $Ct.Po_{US}$ | 0.71 [0.60-0.77] | 1.39 [1.02-1.89]$^{*}$ | **0.035** | 0.65 [0.45-0.76] | 1.35 [0.74-2.46] | 0.312 | 0.84 [0.72-0.90] | 1.96 [1.19-3.23]$^{**}$ | **0.007** | 0.71 [0.58-0.86] | 1.80 [1.01-3.23]$^{*}$ | **0.043** |
| Adjusted aBMD variables | | | | | | | | | | | | |
| aBMD neck | 0.72 [0.64-0.78] | 1.48 [1.00-2.20]$^{*}$ | **0.046** | 0.70 [0.54-0.82] | 1.98 [0.95-4.12] | 0.063 | 0.83 [0.75-0.90] | 1.31 [0.74-2.31] | 0.346 | 0.67 [0.52-0.80] | 1.03 [0.53-2.00] | 0.924 |
| aBMD femur | 0.71 [0.62-0.77] | 1.25 [0.85-1.83] | 0.242 | 0.70 [0.57-0.83] | 2.21 [1.10-4.45]$^{*}$ | **0.023** | 0.82 [0.73-0.89] | 1.17 [0.67-2.05] | 0.574 | 0.67 [0.51-0.80] | 1.23 [0.63-2.42] | 0.538 |
| aBMD spine | 0.70 [0.64-0.77] | 1.05 [0.74-1.49] | 0.775 | 0.64 [0.46-0.78] | 1.21 [0.68-2.14] | 0.504 | 0.83 [0.75-0.90] | 1.16 [0.69-1.96] | 0.565 | 0.69 [0.51-0.83] | 1.44 [0.83-2.50] | 0.188 |
| Adjusted combination of US parameters | | | | | | | | | | | | |
| $Ct.Th_{US}$ | 0.71 [0.61-0.78] | 1.34 [0.95-1.91] | 0.093 | 0.72 [0.57-0.84] | 1.96 [1.16-3.29]$^{**}$ | **0.010** | 0.84 [0.75-0.90] | 1.43 [0.79-2.60] | 0.226 | 0.71 [0.58-0.84] | 1.34 [0.67-2.70] | 0.402 |
| $Ct.Po_{US}$ | | 1.51 [1.08-2.11]$^{*}$ | **0.013** | | 1.14 [0.58-2.22] | 0.701 | | 2.19 [1.27-3.79]$^{**}$ | **0.004** | | 2.03 [1.05-3.93]$^{*}$ | **0.033** |
| Adjusted combination of US parameters and aBMD variables | | | | | | | | | | | | |
| $Ct.Po_{US}$ | 0.73 [0.67-0.81] | 1.41 [1.03-1.93]$^{*}$ | **0.031** | 0.72 [0.57-0.85] | 1.29 [0.71-2.36] | 0.392 | 0.85 [0.76-0.90] | 1.96 [1.19-3.22]$^{**}$ | **0.007** | 0.71 [0.55-0.82] | 1.80 [1.01-3.23]$^{*}$ | **0.043** |
| aBMD neck | | 1.51 [1.01-2.25]$^{*}$ | **0.040** | | 1.95 [0.93-4.09] | 0.073 | | 1.31 [0.73-2.33] | 0.356 | | 1.02 [0.52-1.98] | 0.956 |
| $Ct.Th_{US}$ | 0.71 [0.63-0.77] | 1.16 [0.84-1.62] | 0.357 | 0.74 [0.60-0.86] | 1.92 [1.15-3.19]$^{*}$ | **0.011** | 0.82 [0.75-0.90] | 1.07 [0.66-1.75] | 0.776 | 0.67 [0.47-0.79] | 1.03 [0.58-1.84] | 0.923 |
| aBMD femur | | 1.24 [0.84-1.82] | 0.269 | | 2.14 [1.00-4.57]$^{*}$ | **0.045** | | 1.17 [0.67-2.05] | 0.574 | | 1.23 [0.63-2.42] | 0.536 |

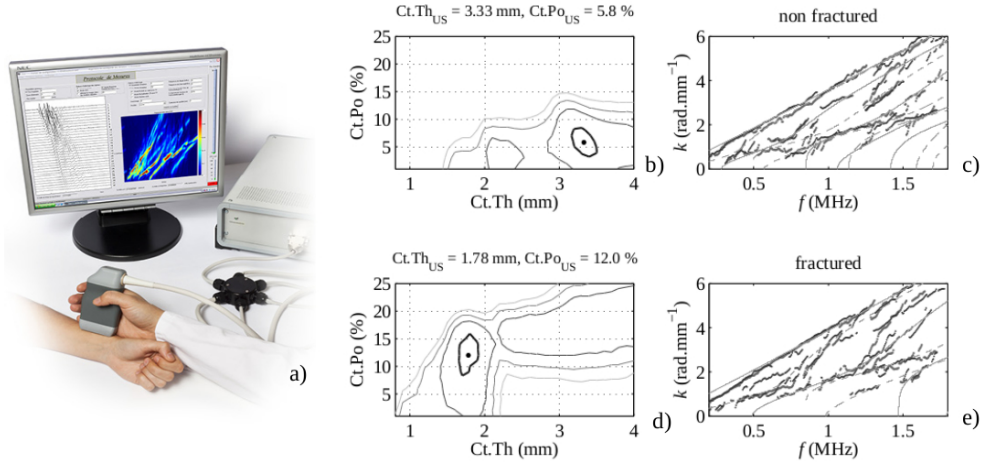


(a) Illustration of the BDAT prototype device placed at the lateral one-third distal radius; (b)-(c) Example of the projected function (Eq. (2)) and guided mode wavenumbers vs frequency for a non-fractured patient; (d)-(e) Example of the projected function (Eq. (2)) and guided mode wavenumbers vs frequency for a patient with a non-traumatic shoulder fracture. The maxima (black dot) of the projected functions shown in (b) and (d) corresponds to the optimal theoretical waveguide models, whose guided modes are shown in (c) and (e) with continuous lines. Experimental guided mode wavenumbers are shown with dots. Contours in (b) and (d) correspond to values equal to the maximum of the projected function minus 0.1, 0.2, 0.3 and 0.4. The area delimited by the highest (thick) line can be interpreted as the measurement resolution, i.e., the ability of the measurement system to differentiate two close waveguide models. The resolution for the two ultrasound parameters is typically estimated to be about ± 0.2 mm and ± 2 %.

277x153mm (100 x 100 DPI)

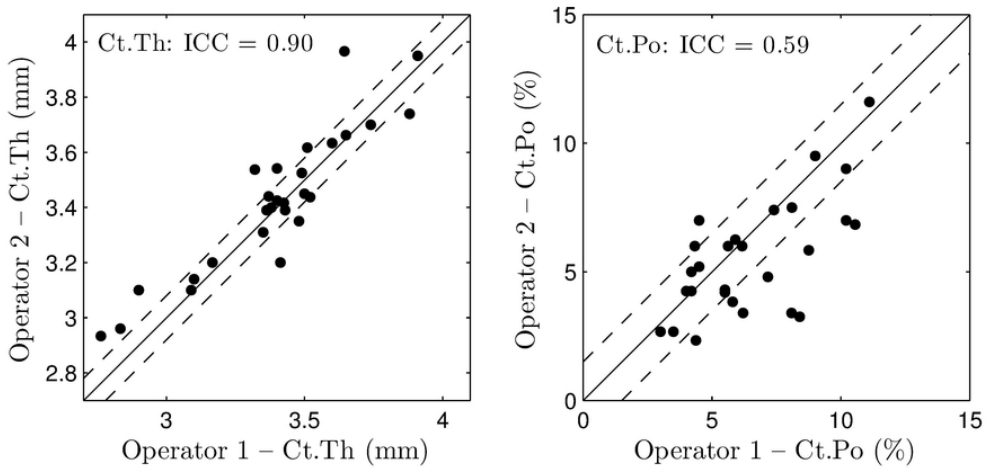


Ct.Th (left) and Ct.Po (right) obtained by the two operators on the 27 healthy subjects of the reproducibility study. Dashed lines correspond to the RMS average of the variance of duplicate measurements, and the ICC is indicated in the upper left corner.

75x36mm (300 x 300 DPI)

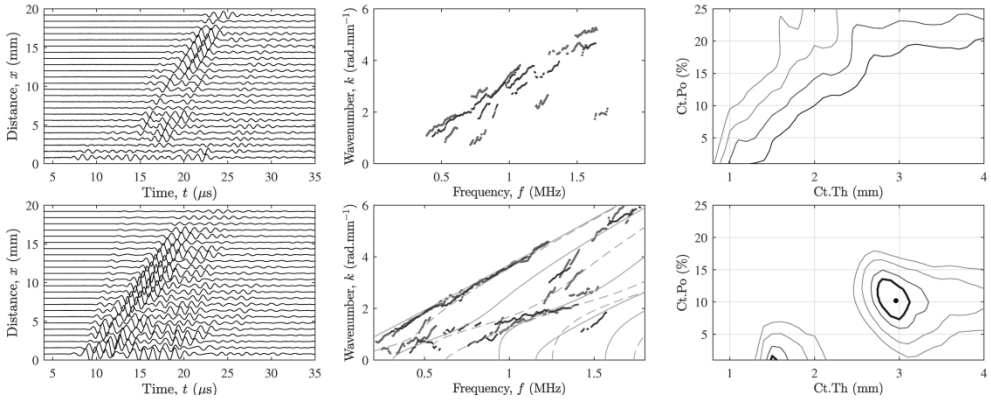


Typical measurements for two patients, corresponding to a failure (upper panels) and a success (lower panels). Three panels are displayed for each measurement: (left) the time-domain signals (for one emission); (middle) the guided modes (*i.e.*, maxima of the *Norm* function); and (right) the projected function (Eq. (2)).

280x110mm (300 x 300 DPI)

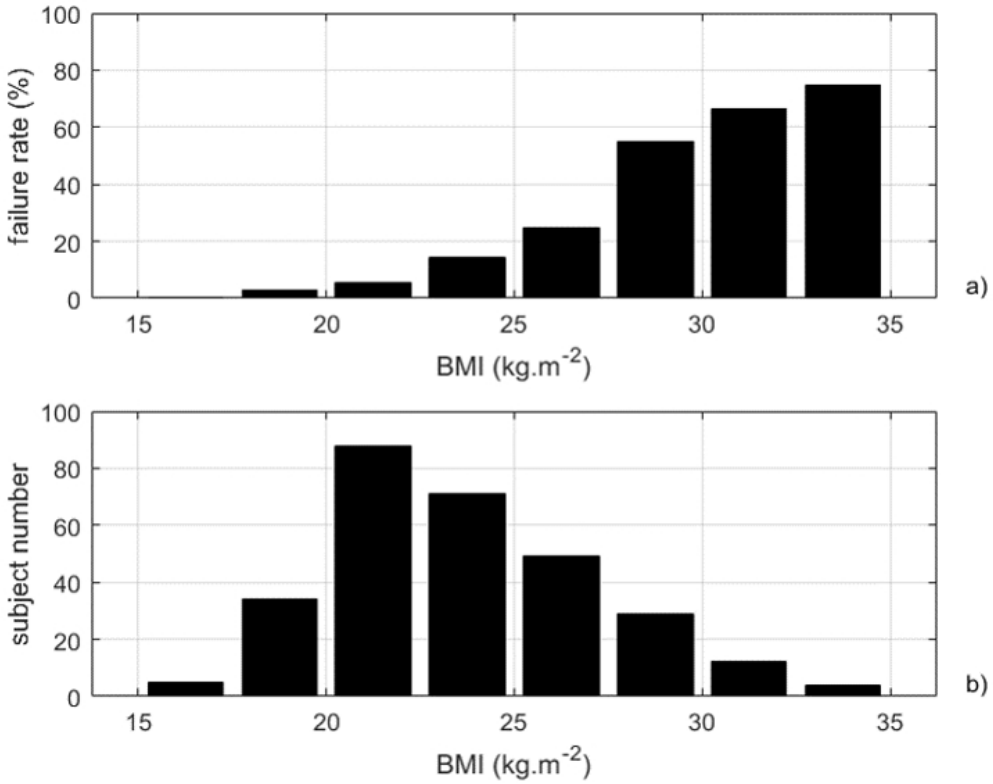


(a) Failure rate (%) vs BMI (kg.m$^{-2}$) and (b) BMI distribution.

174x139mm (105 x 103 DPI)

*Table 3: Odds ratios (ORs) and areas under the ROC curve (AUCs) (Reference category is NF (N=109). CI confidence interval. ROC receiver operating characteristic. AUCs and ORs are adjusted for age, BMI and glucorticoid treatment. The p values of significant results are indicated in bold: *p < 0.05, **p < 0.01, ***p < 0.001).*

| | **All non-traumatic fractures (N=92)** | | | **Hip fractures (N=17)** | | | **Vertebral fractures (N=32)** | | | **Wrist fractures (N=17)** | | |
|---|---|---|---|---|---|---|---|---|---|---|---|---|
| | AUC [95% CI] | OR [95% CI] | *p* | AUC [95% CI] | OR [95% CI] | *p* | AUC [95% CI] | OR [95% CI] | p | AUC [95% CI] | OR [95% CI] | *p* |
| **US parameters** | | | | | | | | | | | | |
| $Ct.Th_{US}$ | 0.63 [0.56-0.71] | 1.46 [1.09-1.94]** | **0.008** | 0.72 [0.59-0.83] | 1.92 [1.22-3.01]** | **0.004** | 0.62 [0.51-0.71] | 1.36 [0.92-2.01] | 0.113 | 0.60 [0.47-0.75] | 1.25 [0.76-2.05] | 0.375 |
| $Ct.Po_{US}$ | 0.62 [0.55-0.69] | 1.47 [1.12-1.95]** | **0.005** | 0.56 [0.39-0.71] | 1.28 [0.74-2.21] | 0.359 | 0.70 [0.59-0.80] | 2.02 [1.34-3.05]*** | **$<10^{-3}$** | 0.69 [0.57-0.82] | 1.97 [1.14-3.42]* | **0.014** |
| **aBMD variables** | | | | | | | | | | | | |
| aBMD neck | 0.65 [0.56-0.72] | 1.88 [1.32-2.66]*** | **$<10^{-3}$** | 0.69 [0.54-0.79] | 1.92 [1.03-3.58]* | **0.035** | 0.64 [0.53-0.75] | 1.86 [1.15-3.03]* | **0.01** | 0.60 [0.42-0.73] | 1.45 [0.81-2.61] | 0.203 |
| aBMD femur | 0.61 [0.52-0.68] | 1.59 [1.15-2.19]** | **0.004** | 0.68 [0.53-0.79] | 2.07 [1.15-3.73]* | **0.014** | 0.59 [0.48-0.68] | 1.41 [0.91-2.18] | 0.112 | 0.55 [0.40-0.69] | 1.20 [0.69-2.10] | 0.503 |
| aBMD spine | 0.52 [0.44-0.60] | 1.10 [0.80-1.51] | 0.542 | 0.57 [0.44-0.71] | 1.12 [0.66-1.92] | 0.659 | 0.56 [0.42-0.66] | 1.30 [0.84-2.02] | 0.236 | 0.53 [0.37-0.71] | 1.17 [0.70-1.97] | 0.541 |
| **Adjusted US parameters** | | | | | | | | | | | | |
| $Ct.Th_{US}$ | 0.70 [0.62-0.77] | 1.18 [0.85-1.63] | 0.317 | 0.72 [0.51-0.85] | 2.01 [1.22-3.33]** | **0.005** | 0.82 [0.75-0.89] | 1.07 [0.66-1.75] | 0.777 | 0.67 [0.49-0.80] | 1.02 [0.57-1.82] | 0.939 |
| $Ct.Po_{US}$ | 0.71 [0.60-0.77] | 1.39 [1.02-1.89]* | **0.035** | 0.65 [0.45-0.76] | 1.35 [0.74-2.46] | 0.312 | 0.84 [0.72-0.90] | 1.96 [1.19-3.23]** | **0.007** | 0.71 [0.58-0.86] | 1.80 [1.01-3.23]* | **0.043** |
| **Adjusted BMD variables** | | | | | | | | | | | | |
| aBMD neck | 0.72 [0.64-0.78] | 1.48 [1.00-2.20]* | **0.046** | 0.70 [0.54-0.82] | 1.98 [0.95-4.12] | 0.063 | 0.83 [0.75-0.90] | 1.31 [0.74-2.31] | 0.346 | 0.67 [0.52-0.80] | 1.03 [0.53-2.00] | 0.924 |
| aBMD femur | 0.71 [0.62-0.77] | 1.25 [0.85-1.83] | 0.242 | 0.70 [0.57-0.83] | 2.21 [1.10-4.45]* | **0.023** | 0.82 [0.73-0.89] | 1.17 [0.67-2.05] | 0.574 | 0.67 [0.51-0.80] | 1.23 [0.63-2.42] | 0.538 |
| aBMD spine | 0.70 [0.64-0.77] | 1.05 [0.74-1.49] | 0.775 | 0.64 [0.46-0.78] | 1.21 [0.68-2.14] | 0.504 | 0.83 [0.75-0.90] | 1.16 [0.69-1.96] | 0.565 | 0.69 [0.51-0.83] | 1.44 [0.83-2.50] | 0.188 |
| **Adjusted combination of US parameters** | | | | | | | | | | | | |
| $Ct.Th_{US}$ | 0.71 [0.61-0.78] | 1.34 [0.95-1.91] | 0.093 | 0.72 [0.57-0.84] | 1.96 [1.16-3.29]** | **0.010** | 0.84 [0.75-0.90] | 1.43 [0.79-2.60] | 0.226 | 0.71 [0.58-0.84] | 1.34 [0.67-2.70] | 0.402 |
| $Ct.Po_{US}$ | | 1.51 [1.08-2.11]* | **0.013** | | 1.14 [0.58-2.22] | 0.701 | | 2.19 [1.27-3.79]** | **0.004** | | 2.03 [1.05-3.93]* | **0.033** |
| **Adjusted combination of US parameters and aBMD variables** | | | | | | | | | | | | |
| $Ct.Po_{US}$ | 0.73 [0.67-0.81] | 1.41 [1.03-1.93]* | **0.031** | 0.72 [0.57-0.85] | 1.29 [0.71-2.36] | 0.392 | 0.85 [0.76-0.90] | 1.96 [1.19-3.22]** | **0.007** | 0.71 [0.55-0.82] | 1.80 [1.01-3.23]* | **0.043** |
| aBMD neck | | 1.51 [1.01-2.25]* | **0.040** | | 1.95 [0.93-4.09] | 0.073 | | 1.31 [0.73-2.33] | 0.356 | | 1.02 [0.52-1.98] | 0.956 |
| $Ct.Th_{US}$ | 0.71 [0.63-0.77] | 1.16 [0.84-1.62] | 0.357 | 0.74 [0.60-0.86] | 1.92 [1.15-3.19]* | **0.011** | 0.82 [0.75-0.90] | 1.07 [0.66-1.75] | 0.776 | 0.68 [0.52-0.82] | 1.03 [0.58-1.84] | 0.923 |
| aBMD femur | | 1.24 [0.84-1.82] | 0.269 | | 2.14 [1.00-4.57]* | **0.045** | | 1.17 [0.67-2.05] | 0.574 | | 1.23 [0.63-2.42] | 0.536 |